PHILOSOPHICAL TRANSACTIONS OF THE ROYAL SOCIETY A MATHEMATICAL, PHYSICAL & ENGINEERING SCIENCES

Surface Microscopy with Scanned Electron Beams

J. A. Venables, D. R. Batchelor, M. Hanbucken, C. J. Harland and G. W. Jones

Phil. Trans. R. Soc. Lond. A 1986 **318**, 243-257
doi: 10.1098/rsta.1986.0074

Phil. Trans. R. Soc. Lond. A **318**, 243–257 (1986)

Printed in Great Britain

Surface microscopy with scanned electron beams

By J. A. Venables, D. R. Batchelor, M. Hanbücken†, C. J. Harland and G. W. Jones

School of Mathematical and Physical Sciences, University of Sussex, Brighton BN1 9QH, Sussex, U.K.

[Plates 1–4]

A brief review is given of the methods that are available for studying surfaces on a microscope scale. The use of finely focused scanned electron beams is described in detail. Examples are given of Auger and secondary electron spectroscopy and microscopy, and of diffraction techniques. These examples are largely taken from recent work of the authors on Ag layers on bulk single-crystal Si(111), Si(100) and W(110) surfaces, but applications to other materials and to thin films are also discussed. Future developments are briefly outlined.

1. Introduction and review

There are now several techniques available for studying the surfaces of solids on a microscopic scale. Such techniques can be classified in various ways. For example, it is possible to separate different techniques by sample geometry. The point-like geometry of the field ion microscope has realized routinely the highest spatial resolution, while it has not found such widespread use as the bulk-sample geometry of the scanning electron microscope, or the thin-film geometry of the (scanning) transmission electron microscope. A rapidly developing technique, which interestingly combines the point- and bulk-sample geometries is the scanning tunnelling microscope.

One can also classify the techniques by the particles used, both as the probe, and as the detected particle, and by whether energy or momentum (diffraction) analysis is made on these particles, and the energy range involved. The proliferation and sub-division of these techniques in recent years has lead to the use of a wide range of abbreviations in surface science and analytical microscopy. However, the usefulness of an individual technique depends on the details: how well energy can be analysed, how well the probe can be localized, how strong the signal is, etc. Consequently, a global review is almost useless, and we have therefore chosen to limit the scope of this paper severely.

The use of electrons, either as the probe or the detected particle, or both, forms an important subset of the available techniques. Many surface-science techniques use electrons, such as Auger electron spectroscopy (A.e.s.) or reflection high-energy electron diffraction (r.h.e.e.d.). Also, electrons are readily focused to form a fine probe, as in scanning electron microscopy (s.e.m.), or can be used to form an image, as in conventional transmission electron microscopy (c.t.e.m.).

The combination of surface techniques (including ultra-high vacuum (u.h.v.), preparation *in situ*, and energy or other analysers) with electron microscopy in either the s.e.m. or t.e.m.

† Present address: CRMC2-CNRS, Campus Luminy, CASE 913, 13288 Marseilles, France.

geometries has been developed intensively over the last ten years in several laboratories worldwide. Reviews of a few years ago could reasonably address this range of activity (Venables 1981, 1982); these articles form a starting point for information about the field as a whole.

Since then the various groups involved have had occasion to write their own reviews. Surface-sensitive c.t.e.m. is described by Yagi (1982), Takayanagi (1982) and Poppa (1983, 1984). These techniques have been particularly successful in providing high-resolution images of monolayer islands and steps, combined with structural information from the diffraction pattern. The application of high-resolution c.t.e.m. (h.r.e.m.) to surface structure is described by Smith & Marks (1985*a*, *b*) and Smith (1985). Reactions *in situ* have been followed with better than 1 nm resolution in a number of cases. The clear implication is that this will be pursued dynamically (at up to television (t.v.) rates) at the ultimate microscope resolution approaching 0.2 nm in future, even though radiation damage will severely limit the range of applicability, by using commercial microscopes specially adapted for u.h.v. and t.v. operation (Iijima & Ichihashi 1985). The combination of r.h.e.e.d. with c.t.e.m. has been as spectacularly successful as reflection electron microscopy (r.e.m.). Images of steps, emergent dislocations, and surface reconstructions, phase transitions and reactions have been seen with great clarity on suitably flat metal and semiconductor surface (Yagi 1982; Yagi *et al.* 1982; Shimizu *et al.* 1985). Some of these features (steps, dislocations) survive transport through the atmosphere, so that r.e.m. can be effected on such features in a conventionally pumped system (Hsu 1983; Hsu & Cowley 1985). Mirror electron microscopy (m.e.m.) as well as m.e.m.–l.e.e.d. combination machines, also continue to be developed, although the resolution is limited to around 0.1 μm at present, but can probably be improved beyond this (Bauer 1985).

Scanning tunnelling microscopy (s.t.m.) is the most recent addition to the armoury of techniques for studying surfaces (see Binnig & Rohrer (1984) for a review), which has attracted much attention. Because it uses low-energy electrons that tunnel between a fine point and a 'planar' surface, it can clearly be classified as a form of electron microscopy. But unlike s.e.m. or t.e.m., which use long-range beam transport, and so are limited by (magnetic) lens aberrations and Fraunhofer diffraction at wavelength λ (the Heisenberg uncertainty principle), s.t.m. uses no lenses and samples the near-field of the tip-sample combination. It is not clear yet whether the resolution (currently under 0.5 nm laterally, and an astonishing 0.01 nm vertically, if the raw results are correct) will be limited by practical or theoretical considerations. But it is interesting that the corresponding optical device (a pinhole 'stethoscope') has achieved resolutions down to less than $\frac{1}{20}\lambda$ (Pohl *et al.* 1984). But independently from resolution, there is an emerging concern about what is actually being measured (see Baratoff 1984 and references quoted therein). This is a long stage, which all analytic techniques pass into (if not through) on the way to becoming fully established.

Because of all these rapid developments, we are limiting this review to topics within our reasonably direct experience, concentrating on s.e.m.-based techniques that use the bulk-sample geometry. In particular, the figures are examples taken exclusively from our own work, which have not been used in previous reviews. Work that can be compared to ours is, of course, being undertaken elsewhere, and we comment on it in the text. Examples are given of secondary-electron imaging in §2, and Auger electron spectroscopy and imaging, in §3. Section 4 is concerned with secondary-electron spectroscopy, and a simple new technique, biased secondary-electron imaging, while §5 is a discussion of diffraction techniques. Scanning transmission techniques are outlined in §6, and the final section, 7, briefly comments on future developments.

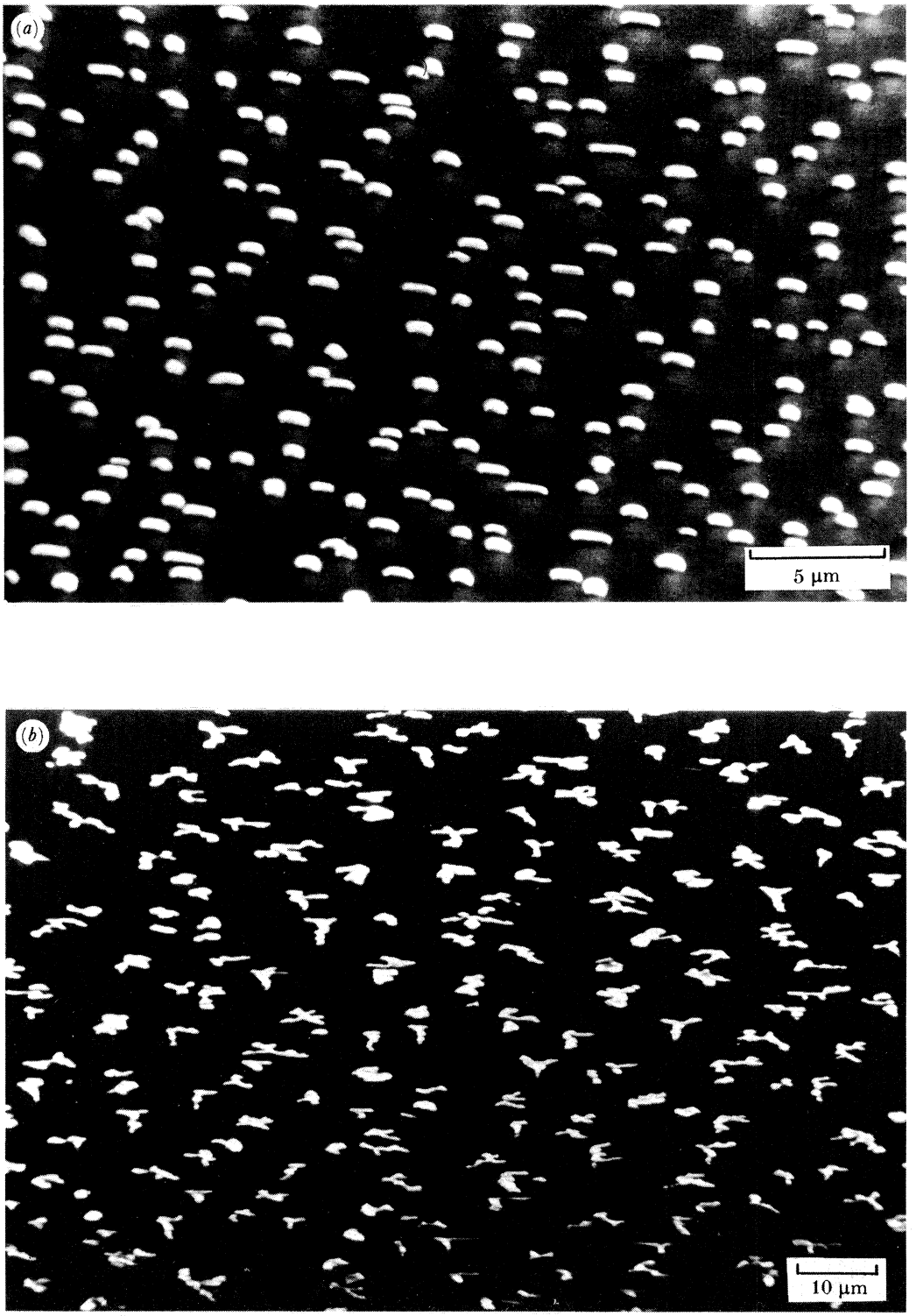

FIGURE 1. S.e.m. pictures of island densities and crystal shapes for (*a*) Ag/Si(100) at $T = 823$ K and (*b*) Ag/Si(111) at $T = 673$ K. Note the higher density on Si(100) despite the higher T, and the difference of shape between the two surfaces. S.e.m. pictures taken at a beam voltage $E_0 = 30$ keV, at $\theta_0 = 70°$ (Hanbücken *et al.* 1984*b*).

(*Facing p.* 244)

PHILOSOPHICAL TRANSACTIONS OF THE ROYAL SOCIETY A MATHEMATICAL, PHYSICAL & ENGINEERING SCIENCES

PHILOSOPHICAL TRANSACTIONS OF THE ROYAL SOCIETY A MATHEMATICAL, PHYSICAL & ENGINEERING SCIENCES

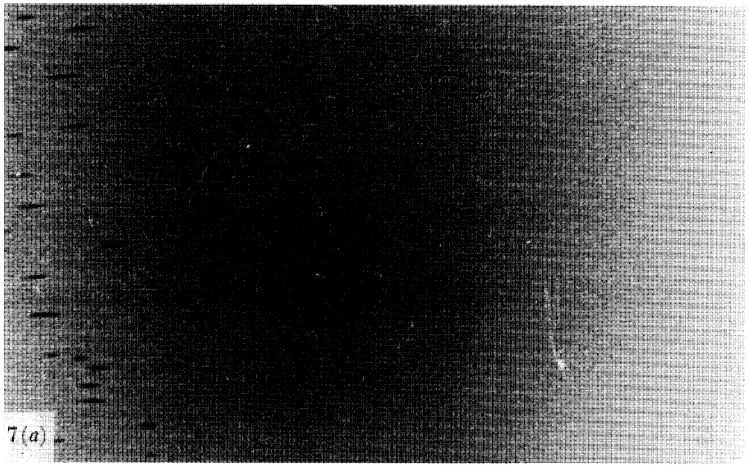

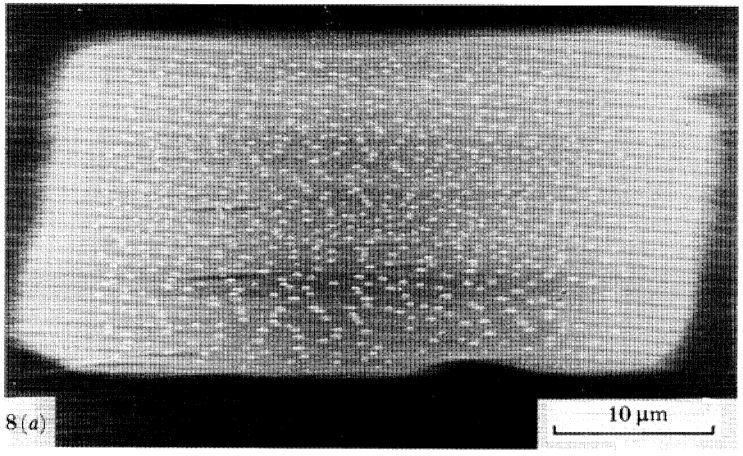

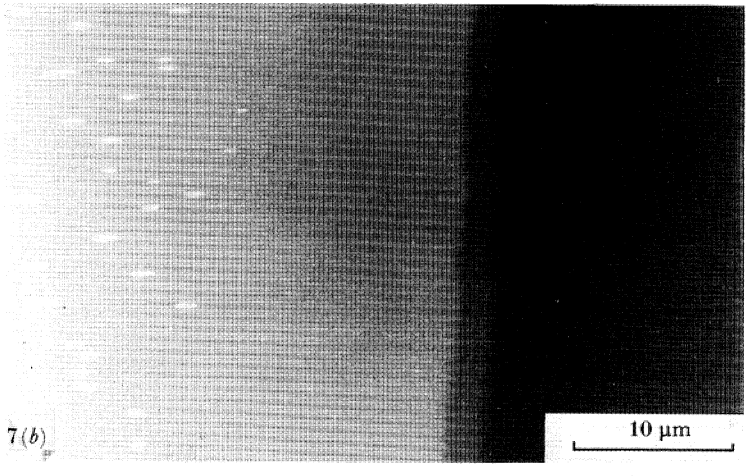

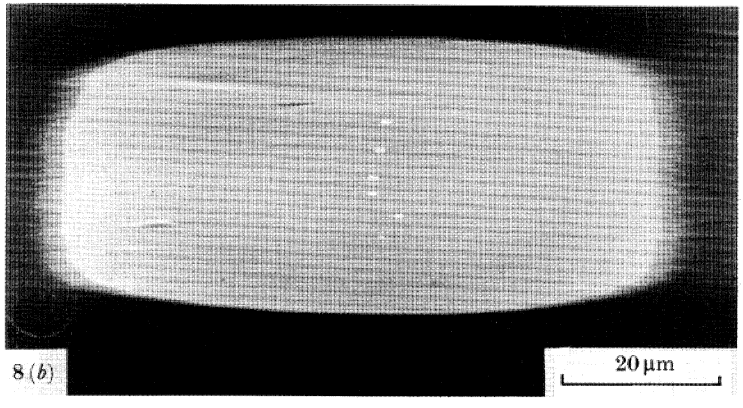

FIGURE 7. Biased secondary-election images of 5 m.l. Ag/W(110), deposited past a mask edge at $T = 673$ K at 0.5 m.l. per minute; observations at $E_0 = 30$ keV, $\theta_0 = 70°$: (*a*) zero bias with the Ag islands showing dark, where the layers are essentially invisible; (*b*) $V_b = -200$ V, showing the islands bright and the 1 and 2 m.l. steps clearly visible (Jones & Venables 1985).

FIGURE 8. Competition between surface diffusion and nucleation on an individual masked area for Ag/W(110). Five monolayers were deposited through a mask hole 32 μm wide by 100 μm long, observed at $E_0 = 30$ keV: (*a*) $T = 573$ K, $\theta_0 = 76°$, diffusion width about 4 μm; (*b*) $T = 733$ K, $\theta_0 = 68°$, diffusion width about 38 μm; (Jones & Venables 1985).

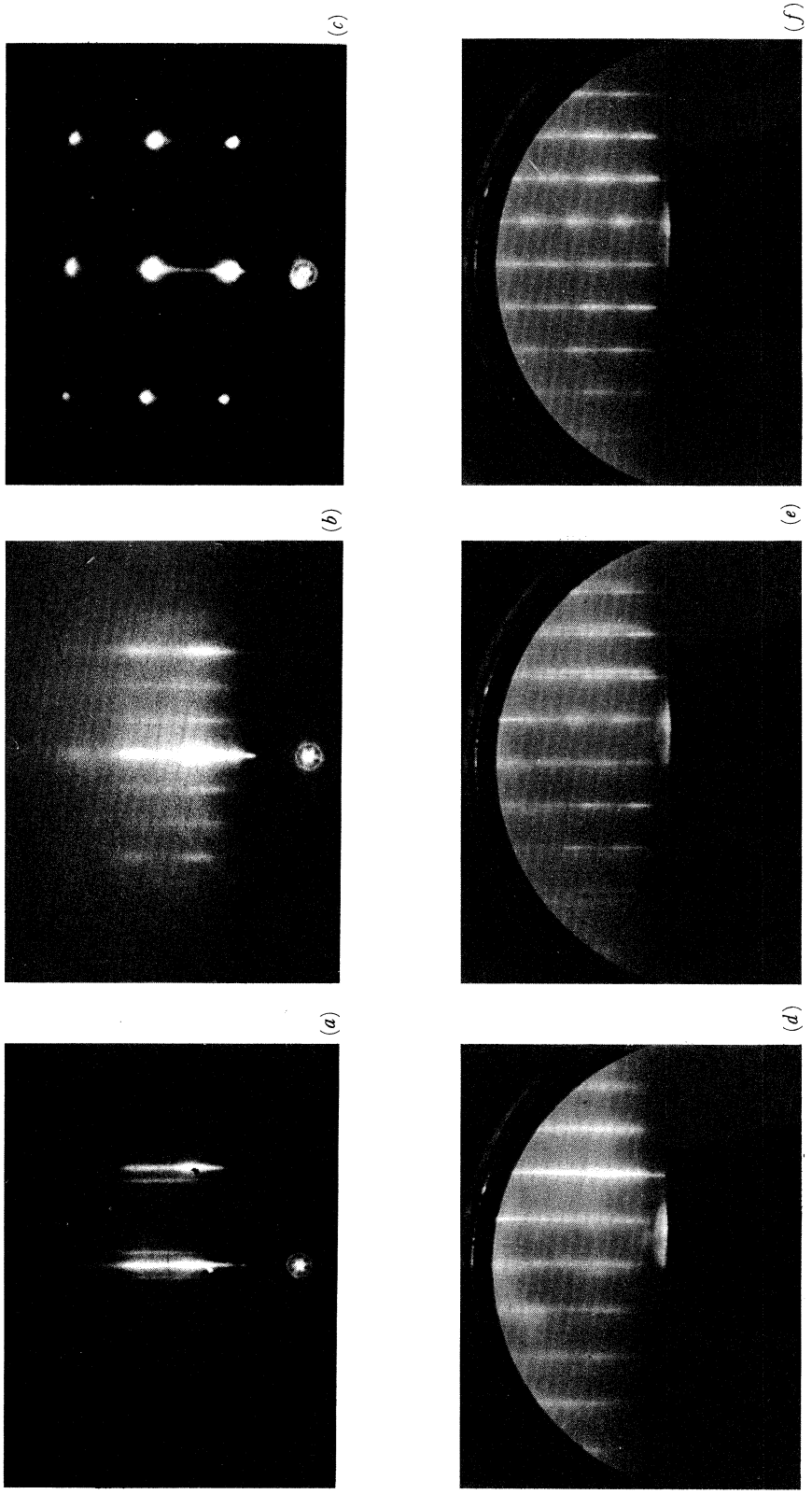

FIGURE 11 R.h.e.e.d. patterns from Ag/Si(111) and Ag/W(110). (*a*)–(*c*) Ag/Si(111) from Venables *et al.* (1980): (*a*) clean Si(111) (7 × 7) veiwed along [11$\bar{2}$]; (*b*) the $\sqrt{3} \times \sqrt{3}$ Ag intermediate layer structure; (*c*) transmission through Ag(111) islands in $\langle 11\bar{2} \rangle$ orientation. (*d*)–(*f*): Ag/W(11) from Jones & Venables (1985): (*d*) clean W(110) viewed along [001]: (*e*) W(110) + 2 m.l. Ag in the 'selvedge' region of figure 7; (*f*) Ag island region showing modulated streaks, corresponding to twinned $\langle 1\bar{1}0 \rangle$ directions.

PHILOSOPHICAL TRANSACTIONS OF THE ROYAL SOCIETY A MATHEMATICAL, PHYSICAL & ENGINEERING SCIENCES

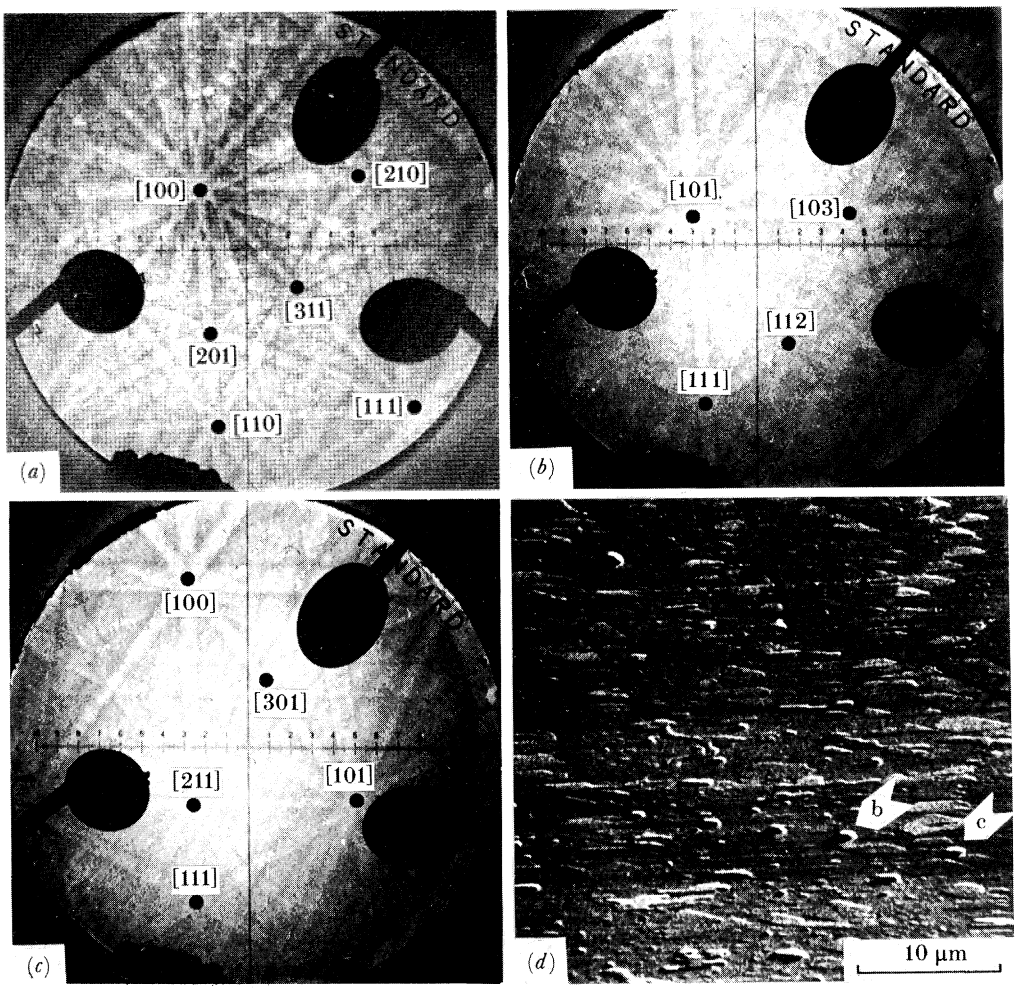

FIGURE 12. Electrons back-scattering patterns from Ag/W(110): (*a*) W(110) substrate patterns; (*b*) (111) oriented Ag crystal; (*c*) similar (111) crystal in twin-related orientation; (*d*) s.e.m. picture at $\theta_0 = 75°$, showing Ag crystals B and C whose patterns are seen in (*b*) and (*c*) respectively (Harland *et al.* 1981).

PHILOSOPHICAL TRANSACTIONS OF THE ROYAL SOCIETY A MATHEMATICAL, PHYSICAL & ENGINEERING SCIENCES

2. Scanning electron microscopy of surfaces

S.e.m. is perhaps the easiest microscopic technique to combine with surface studies. In a crude form it is a standard attachment to A.e.s., r.h.e.e.d. or l.e.e.d. instruments. Several companies now offer u.h.v.–s.e.m. columns, which can operate at or below 50 nm resolution, and which are compatible with other surface facilities. A dedicated u.h.v.–s.e.m. column, such as our own (Venables *et al.* 1980, 1983), which can function at around 10 nm resolution (Venables & Janssen 1980) is still rather better than any commercially available, although comparable resolution is obtainable on non-u.h.v. commercial machines, at sufficiently low probe currents.

S.e.m. pictures enable easy recognition and counting of topographic features such as three-dimensional crystals or etch pits. An example of Ag crystals grown on Si(100) and on Si(111) is shown in figure 1, plate 1, (Hanbücken *et al.* 1984*b*). The crystal shapes are clearly very different on the two substrates, as is their density on the surface. Simple analysis of the s.e.m. images of crystals produced at different temperatures and deposition rates leads to values of nucleation density that can be interpreted in terms of nucleation theories (Venables 1983; Venables *et al.* 1984*a*). More involved, but still essentially topographic, data analysis can use the same pictures to obtain size and spatial distributions (Harland & Venables 1985). Standard s.e.m. detection is useful because one obtains a strong signal, intuitively interpretable in most cases, with a simple detector.

If the sample is not too reactive, topographic information is likely to be preserved on transfer through the atmosphere. In this case, examination by conventional s.e.m. after a surface science preparation, or experiment, is most advantageous. An example of where s.e.m. has been used as a quantitative tool is provided by the measurement of surface energy anisotropy, and adhesion energies, of Au/graphite, Pb/graphite and Pb/Ge(111). In these experiments (Heraud & Métois 1980, 1983; Métois & Lelay 1983), the shape of the crystals was examined in profile, and the Wulff plot evaluated as a function of the treatment temperature, to yield surface energies and entropies of low-index faces, and adhesion energies with the substrate. In other cases, examination by s.e.m. would enable the scientist studying surfaces to check whether his model of the system studied is sufficient; typically, features such as etch pits or surface steps escape notice in wide-beam studies (see, for example, Hanbücken *et al.* 1984*a*). Also, multiple phases may occur, and their properties are averaged by most techniques; an example is the continued discussion over the exact coverage of the Ag/Si(111) $\sqrt{3} \times \sqrt{3}$ structure. Analysis of surface-science experiments based on assumed homogeneity of the samples are likely to be viewed with increasing suspicion in future.

The theory of secondary-electron emission has a long history (Seiler 1984; Kanaya & Ono 1984). The topographic contrast in bulk-sample s.e.m. arises in general from the increased yield at glancing incidence, coupled with the collector geometry. In materials of low atomic number most of the secondaries are produced in the neighbourhood of the incident probe, and it is these electrons that give the high-resolution signal, which can approach 1–2 nm with suitably fine probes, even though back-scattered electrons produce secondaries over a much wider area. The ultimate resolution is beginning to be tested in the new generation of s.t.e.m. machines, where the secondary-electron signal can be compared with the elastic scattering signals used for the highest resolution microscopy; apparently the secondary-electron resolution is not that inferior (Howie & Milne 1985).

Low-energy secondary electrons originate up to around 10 nm below the surface and have

to cross the surface barrier to be detected. These effects give secondary electrons an intrinsic surface sensitivity, which we have explored over the last few years. Because secondary electrons form a strong signal, which can be substantially influenced by surface effects, we give a fuller discussion in §4.

3. Auger electron spectroscopy and microscopy

A.e.s., and its microscopic counterpart scanning Auger microscopy (s.a.m.), are now well established techniques, which have been reviewed many times (see, for example, Venables & Janssen 1978; Browning & Prutton 1979; Venables & Fathers 1982; Prutton 1982). Applied on a microscope scale, point a.e.s analysis can detect the coexistence of several phases, or other gradations in composition. For example, we have shown that we can detect intermediate layers on surfaces between islands, as illustrated in figure 2 for Ag/Si(100) and Ag/Si(111), corresponding to the islands of figure 1 (Hanbücken *et al.* 1984*b*).

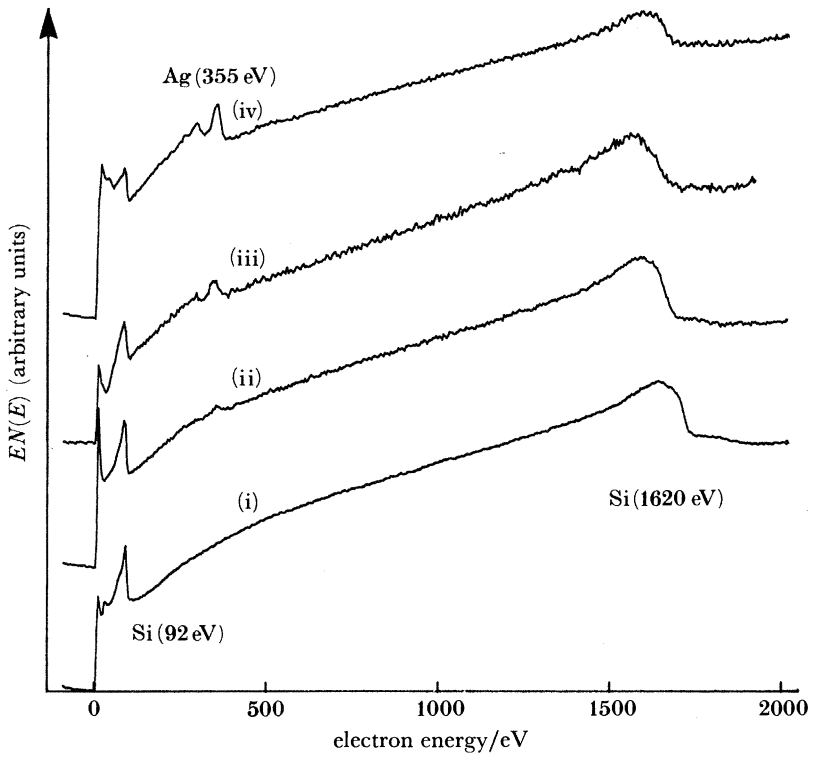

Figure 2. Micro-Auger $EN(E)$ spectra obtained after high-temperature deposition of Ag at $T = 823$ K onto Si(100), and at $T = 623$ K onto Si(111). The spectra show (i) clean Si; (ii) and (iii) Ag(100) and Ag(111), respectively, between the islands; (iv) Ag/Si(100) on an island. Spectra taken at $E = 30$ keV with beam currents in the range 10^{-8} to 10^{-7} A: signal averaged for 150 s (Hanbücken *et al.* 1984*b*).

The Auger peak heights can be analysed quantitatively as function of the experimental variables, in this case the Ag coverage and deposition temperature, as illustrated in figure 3. The quantification procedure is indicated in figure 3*a* (Harland & Venables 1985). The spectra were seen to cross in the region C of the spectrum at all coverages studied; this was used to scale uncalibrated spectra. Least-squares polynomial fits were made to the peak (region A,

third-degree fit) and to the background (region B, second-degree fit); the peak minus the extrapolated background was used as a measure of peak height, as plotted in figure 3*b* for Ag/Si(100). This data gave the first strong evidence for the existence of an intermediate layer in this system at elevated temperatures: its thickness was measured as 0.27 ± 0.03 m.l., where one monolayer (m.l.) is 6.8×10^{14} atoms per square centimetre for Si(100).

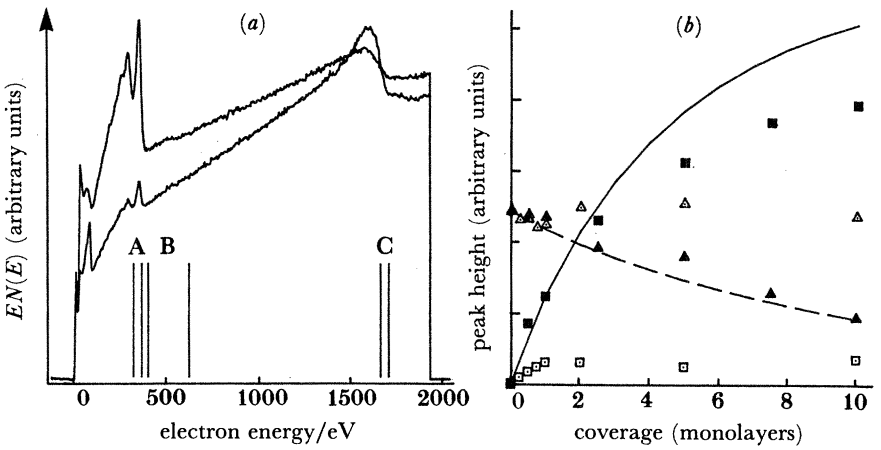

FIGURE 3. Quantification of micro-Auger signals for Ag/Si(100): (*a*) spectra from 0.5 and 10 m.l. room-temperature deposits, showing Ag peak (A), background (B) and calibration (C) regions of interest (see text for discussion); (*b*) Ag and Si peak heights from the layers against versus coverage at two deposition temperatures: $T = 293$ K (room temperature), solid squares (Ag) and triangles (Si); $T = 773$ K, open symbols. The full and broken lines are numerical layer-growth calculations, made by using a mean free path $\lambda = 0.82$ nm for Ag (355 eV) and 1.90 nm for Si (1620 eV) Auger electrons. The higher T data are interpreted as an intermediate layer thickness of 0.27 ± 0.03 m.l. (see text for discussion). (Hanbücken *et al.* 1984*b*, Harland & Venables 1985.)

Such data processing is an essential feature of extracting the maximum elemental sensitivity from the relatively weak A.e.s. signal when it is applied on a microscope scale. Probe currents are typically in the 1–10 nA range, with data collection times around 150 s per spectrum for our equipment. The use of the undifferentiated pulse-counted $E\,N(E)$ or $N(E)$ signal plus the background subtraction has clearly gained ground over the last few years, both for reasons of sensitivity, and because the background itself contains information that is lost in conventional differential techniques. The form of the background, and its dependence on instrumental and sample variables has been studied by ourselves (Batchelor *et al.* 1984, 1985) and others (Bishop 1982, 1984; Peacock *et al.* 1984). The use of a power-law background $N(E) \sim A\,E^{-r}$ (Sickafus 1977; Peacock *et al.* 1984) is finding favour, though orthogonal polynomials are equivalent over sufficiently small energy windows, and are very simple to use.

Although the basic Auger equations are well known, a first-principles quantification depends on a detailed knowledge of ionization cross sections σ and Auger branching ratios γ matrix-dependent back-scattering factors R and mean free paths λ as well as instrumental variables. The combined effect of all these variables makes quantitative A.e.s. and s.A.m. difficult in general, even with standards (Prutton 1982; Browning *et al.* 1985); considerably different peak heights have been obtained in 'round-robin' experiments between different laboratories (Powell *et al.* 1982), particularly for low-energy peaks.

As a step towards the quantification of $N(E)$-based Auger signals, we have taken Auger

spectra from several elements (C, Si, V, Cu, Ag, W, Au) across the periodic table in two separate s.A.m. machines (Batchelor *et al.* 1984, 1985). Peak (P) and background (B) heights have been measured as a function of beam energy E_0 and angle of incidence θ_0. The energy dependence at a given angle in the range $2 < E_0 < 30$ keV, measures the combination (σR); the angle dependence is dominated by the (calculable) analyser acceptance, but once this is accounted for, there is a variation $R(\theta_0)$ in addition, which varies in opposite ways for materials of high and low atomic number (Fathers & Rez 1984; El Gomati *et al.* 1983; Batchelor 1985).

Of the large amount of data collected, we show two figures of interest for micro-A.e.s. and s.A.m. Figure 4 shows the ratio P/B as a function of θ_0, taken in the VG MA 500 machine at Harwell. This ratio depends on the energy resolution of (and any background signals in) the analyser, but is largely independent of θ_0 for all but glancing angles. Such a signal can therefore be used approximately for s.A.m. in the presence of surface topography variations, as originally explored by Janssen *et al.* (1977), and subsequently implemented digitally on several machines.

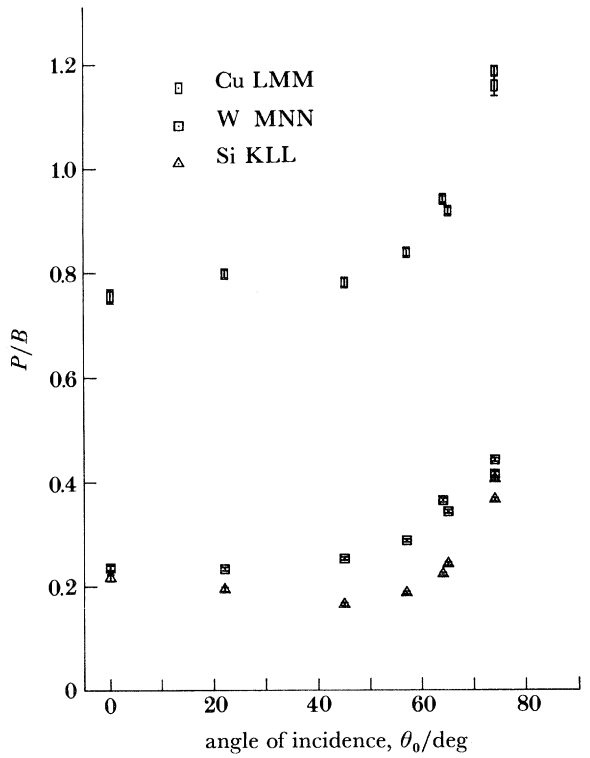

FIGURE 4. Peak: background (P/B) ratio as a function of incidence angle, θ_0, at $E_0 = 10$ keV, for the high-energy Auger transitions Si (1620 eV), Cu (914 eV) and W (1730 eV). The spectra were taken on the VG MA500 machine at Harwell (Batchelor 1985).

The ratio $P/B^{\frac{1}{2}}$ is a measure of detectability and is shown as a function of E_0 in figure 5. Whereas the peak height, P, has a maximum at an overvoltage ratio $U = E_0/E_I$ around 4–5, where E_I is the ionization energy of the shell concerned, $P/B^{\frac{1}{2}}$ is maximum at U around 8–10. This, plus electron-optical reasons, tend to favour higher voltage operation for s.A.m. machines than would be expected on the grounds of peak height alone (Bishop 1982); choices in the range

10–30 keV are presently sensible. In addition, backgrounds become flatter with increasing E_0, which facilitates background fitting and the use of simpler algorithms for forming images.

It is now recognized that Auger images (maps) and line-scans cannot be obtained simply by fixing the analyser energy at the Auger peak energy E_A and scanning the probe, because the background also varies and, in field-emission gun machines, the probe current is rather unstable. The procedure that we have adopted (Harland & Venables 1985) is to collect images

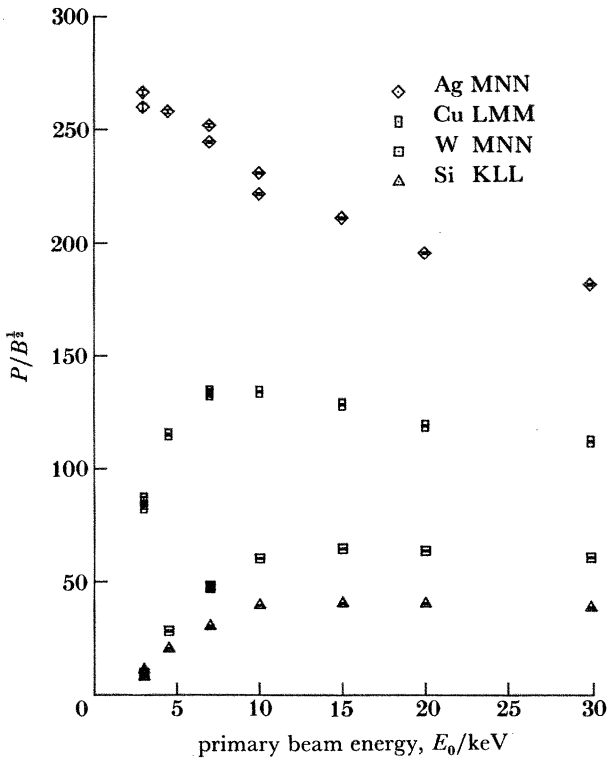

FIGURE 5. $P/B^{\frac{1}{2}}$ ratio as a function of beam energy, E_0, for an incident angle $\theta_0 = 65°$, for Si, Cu, W and in addition, Ag (345 eV). The incident electron dose was scaled to 10 nC, to give absoulte peak and background counts before forming the ratio (Batchelor 1985).

at three energies, A on the peak and B and C equally spaced on the background at higher energies. Data processing then produces the Auger map, which one hopes gives just the element distribution. The most widely used algorithm is $(A-B)/(A+B)$, which is the simplest digital equivalent of the logarithmic derivative $N'(E)/N(E)$ at an energy $\frac{1}{2}(A+B)$. This has been used by several authors (Janssen *et al.* 1977; Hovland *et al.* 1979; Prutton 1982; Harland & Venables 1985).

The alternative signal we have used is $(A-2B+C)/(2B-C)$, which is the simplest linear measure of the peak: background ratio, allowing the background height and slope to vary from point to point. Both algorithms compensate for beam current fluctuations, although the second one is noisier; the high quality of the individual energy-selected images needed to make adequate Auger maps by these difference techniques has been emphasized by Venables *et al.* (1983) and Fathers *et al.* (1984). Some strategies for dealing with noisy s.A.m. images are

described by Browning *et al.* (1984) and Peacock & Prutton (1984). The use of the P/B ratio has also been advocated by Bishop (1983) and by Langeron *et al.* (1984). However, it is clear that this ratio is only a first approximation to a quantitative signal, and in fact overcompensates for backscattering factor differences (Janssen *et al.* (1977); Batchelor (1985)).

Optimization of the signal:noise ratio for Auger mapping required larger solid-angle collection, and larger energy windows than for high-resolution spectroscopy, with a collection geometry that minimizes topographic effects. Such improvements are part of current design efforts for future instrumentation and quantification routines. Essentially similar developments are taking place in electron energy loss spectroscopy (e.e.l.s.), where the peak:background problem is, if anything, worse, though the signal strength can be higher (see for example, Jeanguillaume *et al.* 1983; Colliex 1984 for reviews).

4. Biased secondary-electron spectroscopy and imaging

A few years ago we explored a technique for making monolayers on surfaces, visible and applied it to Cs layers on W substrates (Janssen *et al.* 1980; Akhter & Venables 1981). This consisted of biasing the sample negatively to around −15 V, and tracking the onset energy

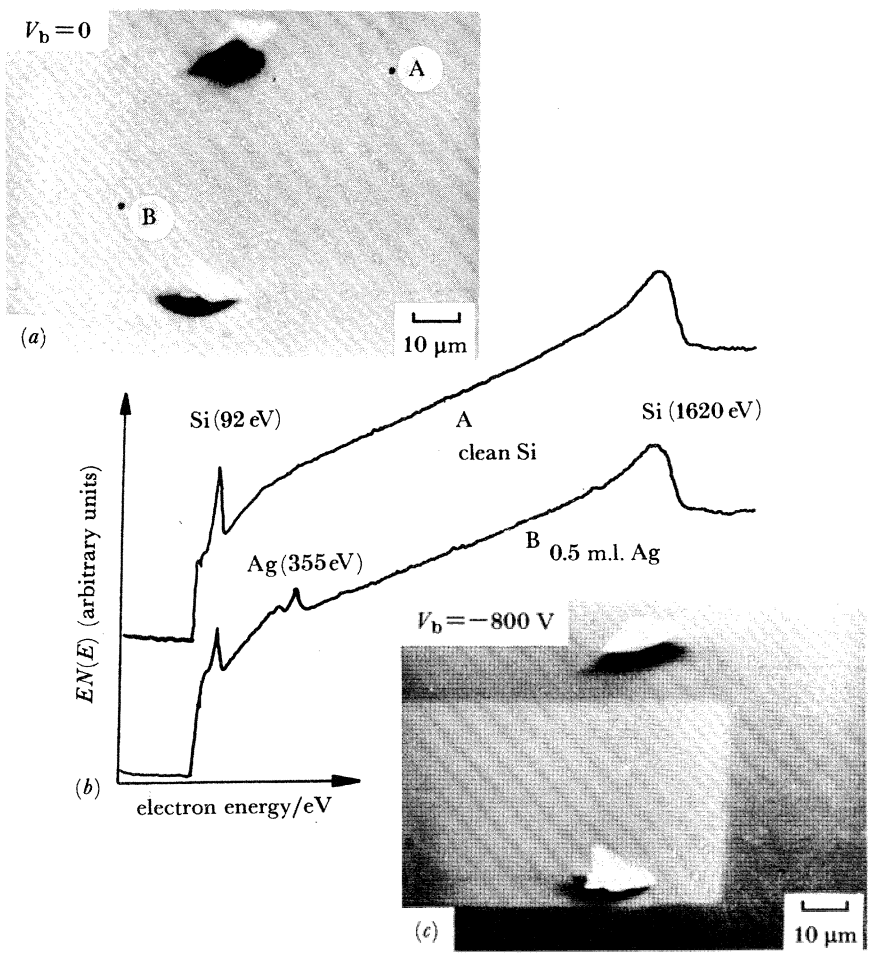

Figure 6. Demonstration of biased secondary-electron imaging for 0.5 m.l. Ag/Si(100), deposited at room temperature. (*a*) zero bias, showing dust-particle markers; (*b*) Auger spectra from points A and B in (*a*); (*c*) sample bias $V_b = -800$ V, showing the masked area of Ag deposited (Futamoto *et al.* 1985).

of the low-energy secondary-electron spectrum to form a surface-potential map. Various effects of patch fields above the surface were seen, but the spatial resolution was shown to be under 0.4 μm with energy resolution of under 40 mev.

More recently an even simpler technique has been developed to make surface layers visible by using secondary electrons (Futamoto *et al.* 1985; Hanbücken *et al.* 1984*b*). This consists of biasing the sample to V_b around -500 V, and using the normal secondary-electron collector. The technique is illustrated in figure 6 for 0.5 m.l. Ag/Si(100). The Ag is evaporated through,

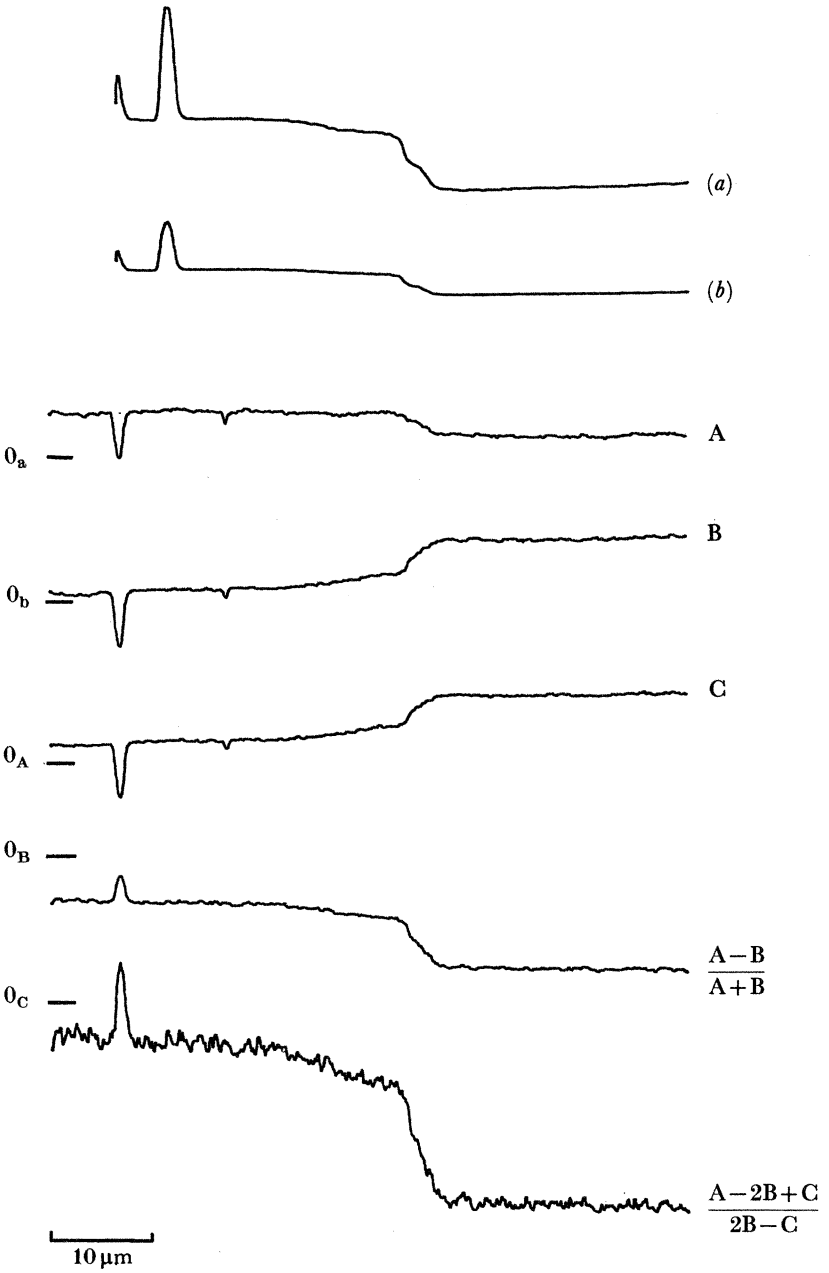

FIGURE 9. Biased secondary-electron and Auger line-scans of the edge corresponding to figure 7. Secondary-electron scans (*a*) and (*b*) with and without zero suppression, respectively. Energy-selected scans $A = 346$ V, $B = 385$ V, and $C = 424$ V. Auger line-scans based on the algorithms $(A-B)/(A+B)$ and $(A-2B+C)/(2B-C)$. See text for discussion (Jones & Venables 1985).

and past the edge of, a mask of holes; the masked area is seen only in the biased image (figure 6*c*), correlating with the presence of Ag in the Auger spectrum (figure 6*b*). More details of the systematic dependencies with angle of incidence, bias and coverage are given by Futamoto *et al.* (1985). The sensitivity has been seen to be under 0.1 m.l. for Ag/Si(111).

An immediate application of this achievement is to surface diffusion, and to the competition between surface diffusion and the nucleation and growth of crystals (Hanbücken *et al.* 1985; Jones & Venables 1985). For Ag/W(110), we know from previous studies on unmasked areas that Ag islands grow on top of two intermediate layers of Ag (Spiller *et al.* 1983). Figure 7 illustrates the edge of the mask area both without and with bias applied, after deposition of 5 m.l. at 673 K. Fig 7*a*, plate 2, shows, under zero bias, that the Ag islands are dark, but the layers are essentially invisible. Figure 7*b*, at $V_b = -200$ V, shows the islands and layers bright and reveals the 1 m.l. and 2 m.l. steps very clearly. The edge has moved substantially due to diffusion; the temperature dependence of diffusion and nucleation on individual masked areas is very marked, as illustrated in figure 8. Detailed analyses of such pictures and line-scans for Ag/Si(111) and Ag/W(110) will be given future publications by the authors.

Quantitative analysis of the diffusion is best achieved by using line-scans. Biased secondary-electron and Auger line-scans are shown in figure 9, corresponding to the mask edge of figure 7. The secondary-electron line scans took much less time to accumulate than the Auger scans, but correspond with them extremely well. The individual energy-selected scans at *A*, *B* and *C* for Ag, and the processed-scans made by using the algorithms discussed in §3, are also shown in figure 9. Note that the changes in background (*B* and *C*) are substantial even for a 2 m.l. thick Ag deposit, and that there is evidence for a more widely diffused third layer in contact with the islands. Similar comparisons of Auger and biased secondary-electron images have been made elsewhere (Futamoto *et al.* 1985; Harland & Venables 1985; Jones & Venables 1985).

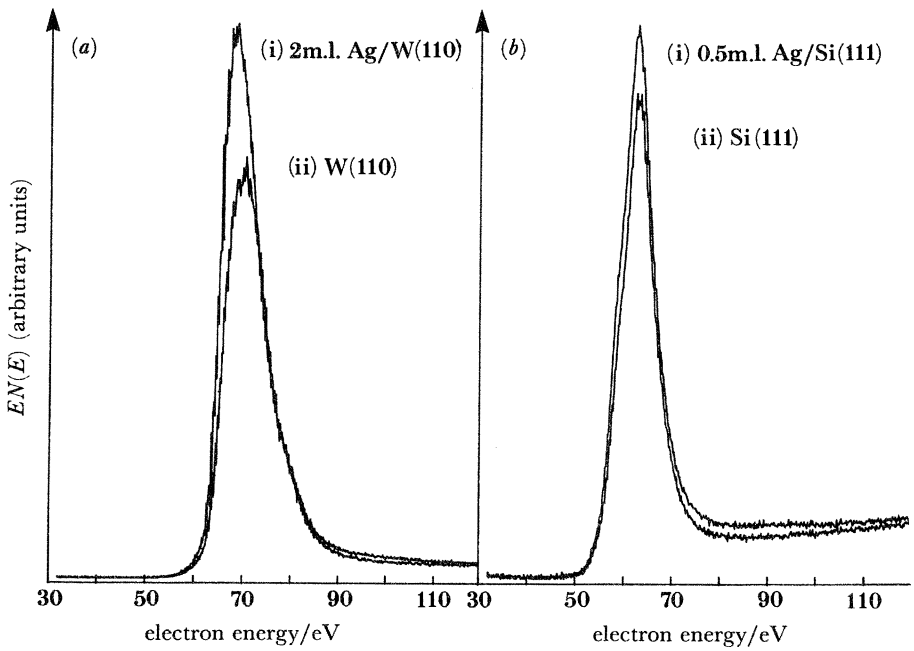

FIGURE 10. Biased secondary-electron spectra for $V_b \approx -50$ V: (*a*) 2 m.l. Ag/W(110) at $\theta_0 = 69°$; (*b*) 0.5 m.l. Ag/Si(111) at $\theta_0 = 67°$. Line (i) is on the deposited patch, line (ii) on the substrate (Futamoto *et al.* 1985).

The contrast mechanisms can be investigated by biased secondary-electron spectroscopy, even though the biasing may distort the analyser response in asymmetrical geometries, such as our own current arrangement, which forces us to use relatively small values of V_b. Examples for Ag/W(110) and Ag/Si(111) are shown in figure 10. For the metal–metal interface the contrast is largely due to the low-energy secondaries, which can escape from the lower work-function Ag-layer ($\Delta\phi \approx -0.75$ V). For the metal–semiconductor interface, the difference between the deposit and the substrate is not confined to the low-energy region, but is spread over the spectrum, corresponding largely to a shift in ionization energy caused by band-bending at the surface. The contrast in these spectra can exceed 10% for 1 m.l. coverage for Ag/Si(111). Such spectra and images clearly have considerable potential for investigating metal–semiconductor interfaces and Schottky barriers.

5. Diffraction techniques at surfaces

There are several diffraction-based techniques that are either surface-sensitive or can be used to obtain surface-related information. Typical intensities of diffracted beams from a monolayer in the transmission geometry are around 10^{-4} to 10^{-3} of the incident beam, both for adsorbed layers (Schabes-Retchkiman & Venables 1981) and for monolayer changes in thickness (Cherns 1974; Spence 1976; Takayanagi 1982). If the samples are turned through almost 90°, and examined in the reflection geometry, the diffracted intensity from the surface layers rises dramatically; this sensitivity to ordered surface layers is exploited in r.h.e.e.d. and r.e.m.

R.h.e.e.d. in a scanned-beam instrument can be used most readily to observe the surface crystallography of particular areas, as illustrated in figure 11, plate 3, for Ag/Si(111) and Ag/W(110). The technique is very sensitive to sub-monolayer deposits and to surface corrugations such as etch pits or islands. For surface corrugations, characteristic transmission patterns are seen, such as those in figure 11*c*; r.h.e.e.d. is thus very useful for identifying the 'layer-plus-island' growth mode, even when the islands cannot be seen directly (see, for example, Venables *et al.* 1984*b*).

To form a scanning reflection (s.r.e.m.) image, the beam is focused onto the sample, which gives a convergent beam pattern on the r.h.e.e.d. screen that can be similar in complexity to the beautiful patterns observed in transmission (Steeds 1983). Use of part of this pattern as a signal was pioneered by Cowley *et al.* (1975) and Hembree & Cowley (1979). More recently, Ichikawa *et al.* (1984) and Bennett *et al.* (1985) have obtained s.r.e.m. images of the Si(111) 7×7 and 2×1 surfaces, respectively. These images are useful as an adjunct to other surface studies, but are not yet as impressive (as pictures) as the conventional r.e.m. images (Osakabe *et al.* 1980; Yagi *et al.* 1982; Tanashiro *et al.* 1983; Hsu 1983; Hsu & Cowley 1984; Shimizu *et al.* 1985). The reason is largely that the simultaneous requirement of a small probe-size and good angular resolution at the detector leads to very small detected currents and, consequently, noisy images; this problem is largely avoided in c.r.e.m. However, there is still room for further instrumental improvement, and for the exploitation of convergent-beam diffraction patterns from surfaces (Shannon *et al.* 1984). The combination of s.e.m., A.e.s. and r.h.e.e.d. in one instrument is very useful, and is finding applications in several laboratories (Venables *et al.* 1980, 1983; Ichikawa & Hayakawa 1982; Ichinokawa & Ishikawa 1984*a*, *b*; Ichikawa *et al.* 1984; El Gomati *et al.* 1985).

Another diffraction technique that is useful in surface studies, although not specifically

surface-sensitive, has been called electron back-scattering patterns (e.b.s.p.). It consists simply of observing the Kikuchi patterns, which occurs at near-glancing incidence (θ_0 around 75°), by viewing a fluorescent screen placed at higher observation angles that the r.h.e.e.d. screen (Harland *et al.* 1981). This technique explores the smallest volume of the crystallographic methods currently available for bulk samples, and accurate epitaxial orientation relations can readily be obtained from many crystals. As illustrated in figure 12, plate 4, and 13 for

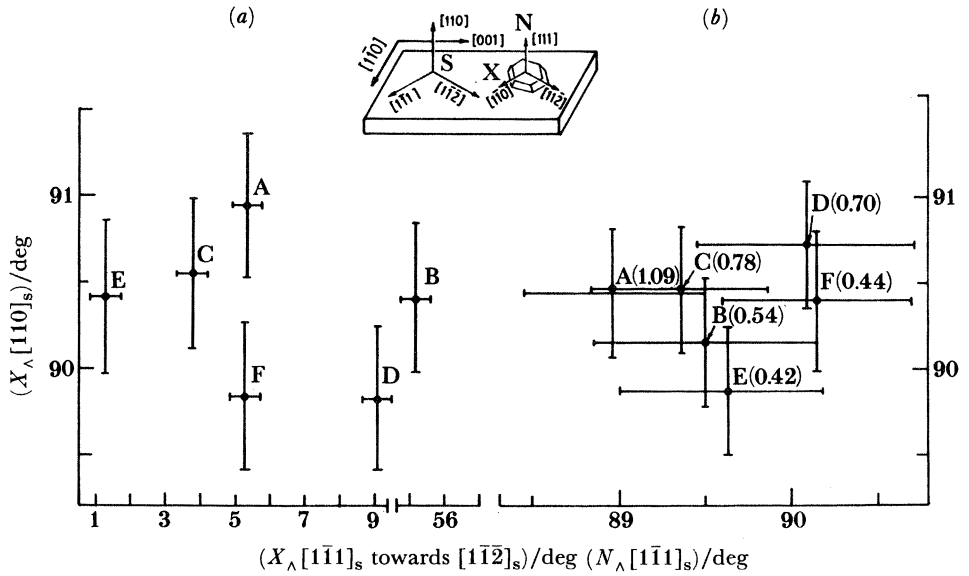

FIGURE 13. Crystallographic analysis of Ag crystals corresponding to figure 12: (*a*) distribution of $X = [1\bar{1}0]$ Ag; (*b*) distribution of $N = [111]$ Ag with respect to axes in the W substrate (S) (values of $N_\wedge[110]$s are given in brackets). Note that [111] Ag is closely parallel to [110] W. but that there is an azimuthal distribution of ±4° around this normal to the substrate, centred on the Nishiyama–Wassermann orientated relation (Harland *et al.* 1981).

Ag/W(110), the Ag(111) planes are accurately parallel (within 0.5°) to W(110), whereas there is a spread of orientations (*ca.* ±4°) about this normal direction. Similar epitaxial orientation-relation determinations are being made presently on other systems, both *in situ* in the u.h.v. environment after deposition, and *ex situ* in a standard s.e.m. It is likely that epitaxial orientation relations will not be altered, in not too reactive systems, during a reasonably rapid transfer through the atmosphere, though this of course needs to be checked in individual cases; there are certainly counter-examples for very small particles (Heinemann *et al.* 1983; Poppa 1984).

6. Scanning transmission techniques

With bulk samples, inelastic scattering processes in the electron cascade limit the spatial resolution obtainable; consequently, the highest resolution pictures are obtained with thin films by using essentially scattered electrons. Understanding of the images is very sensitively linked to a knowledge of defocus and lens aberrations, and a thorough understanding of diffraction by the sample. Recently, however, advances in c.t.e.m. instrumentation and associated computing have led to impressive lattice images (both experimental and calculated), and the work has begun to move in the direction of surface structure (Smith & Marks 1985*a*, *b*; Smith 1985; Iijima & Ishihasi 1985). An example that has been cited in the literature

is the observation of the Au(110) 2×1 structure in profile, confirming the 'missing row' model of this surface (Marks & Smith 1983; Marks 1983).

As explained elsewhere (Cowley & Kang 1983; Cowley 1984), s.t.e.m. instruments offer no particular advantage over c.t.e.m. for high-resolution imaging, but the provision of analytic facilities at around 1 nm is an attractive feature. Studies of diffraction and electron energy loss have been made on individual small particles that are below 5 nm in diameter (Batson 1984; Cowley 1984; Howie & Milne 1985) in reasonably clean vacuum conditions. The design and construction of a fully u.h.v.–s.t.e.m. with surface analytical facilities is a current development project. In particular, it is possible to envisage s.t.e.m. imaging below 0.5 nm combined with A.e.s., e.e.l.s., secondary-electron spectroscopy and imaging at 1–2 nm resolution, by using the spiral focusing properties and excellent collection-efficiency of the high magnetic field for low-energy (under 1 keV) electrons (Beamson *et al.* 1980, 1981; Kruit & Read 1983).

7. Future developements

There has been a recent rapid growth of interest in the examination of surfaces on a microscopic scale. In the separate fields of surface science and analytical microscopy, there have been several developments that have brought the areas together. The developments involving scanned electron beams have been described in this article. Further developments can be envisaged, which are briefly discussed here.

S.e.m.-based examination of bulk samples, coupled with the use of surface analytical signals, will continue to be developed, especially in relatively low-voltage (0.1–30 keV) microscopes. We have a project in progress along these lines, as has Ichinokawa (1984). He has shown that e.e.l.s. from surfaces is very surface-sensitive, as is the back-scattered elastic signal. Opportunities also exist for studying the angular dependence of these various surface spectroscopies and for beam-induced effects (for example electron-stimulated desorption and its angular dependence (Madey *et al.* 1983)) on a microscopic scale. The resolution obtainable will, of course, be limited by signal strength, electron optics and sample damage.

At higher resolution (under 5 nm), s.t.e.m.-based techniques are required, which use 50–150 keV beams, as discussed briefly in §6. An essential feature for low-energy electron spectroscopy will be to use the intrinsic high collection efficiency of the magnetic field at the sample, since this alone can compensate for the reduced excitation of surface-sensitive signals at higher voltages.

Finally, we should see the wider use of such microscopic surface techniques in both academic and industrial research, and in process control. The commercial s.e.m.–A.e.s. instruments are being simplified and more automated, but more specialized as to end use. Similarly, in research laboratories, such equipment will start to take its place as commercially available bolt-on attachments to surface-science chambers, for a wide range of materials experiments. However, the development of the highest peformance surface microscopes, whether s.e.m., c.t.e.m., s.t.e.m. or s.t.m.-based, both alone and in combination with other techniques, will be done in a few laboratories worldwide, at a price that is becoming uncomfortably close to 'big science' costs. Such developments therefore require careful comparisons with other potentially competitive techniques, but, above all, positive plans for the future. It is clear that there is a large amount of fascinating detail about surfaces and surface processes still to be revealed, and that scanned electron beams have a major role to play.

PHILOSOPHICAL TRANSACTIONS OF THE ROYAL SOCIETY A MATHEMATICAL, PHYSICAL & ENGINEERING SCIENCES

We thank the S.E.R.C. for continuing to support this work, and for studentships and fellowships for D. R. Batchelor, M. Hanbücken and G. W. Jones. J. A. Venables thanks the conference organizers for the opportunity to present this paper, several colleagues at Arizona State and Sussex Universities for support and constructive criticism while it was written, and many others for supplying reprints and preprints.

References

Akhter, P. & Venables, J. A. 1981 *Surf. Sci.* **103**, 301–314.
Baratoff, A. 1984 *Physica* B**127**, 143–150.
Batchelor, D. R. 1985 Ph.D. thesis, University of Sussex.
Batchelor, D. R., Bishop, H. E., Fathers, D. J. & Venables, J. A. 1984 In *Inst. Phys. Conf. Ser.* no. 68 (EMAG 1983), pp. 139–142.
Batson, P. E. 1985 *Ultramicroscopy* **18**, 125–130; *Surf. Sci.* **156**, 720–734.
Bauer, E. 1985 *Ultramicroscopy* **17**, 51–56.
Beamson, G., Porter, H. Q. & Turner, D. W. 1980 *J. Phys.* E**13**, 64–66.
Beamson, G., Porter, H. Q. & Turner, D. W. 1981 *Nature, Lond.* **290**, 556–561.
Bennett, P., Ou, H., Elibol, G. & Cowley, J. M. 1985 *J. Vac. Sci. Technol.* A **3**, 1634–1635.
Binnig, G. & Rohrer, H. 1984 *Physica* B **127**, 37–45.
Bishop, H. E. 1982 In *Inst. Phys. Conf. Ser.* no. 61 (EMAG 1981), pp. 435–438.
Bishop, H. E. 1983 In *S.E.M. Proceedings* (ed. O. Johari), vol. 3, pp. 1083–1090.
Bishop, H. E. 1984 In *Electron beam interactions with solids*, pp. 259–269. Asilomar: S.E.M. Inc.
Browning, R., Peacock, D. C. & Prutton, M. 1985 *Appl. surf. Sci.* **22/23**, 145–159.
Browning, R & Prutton, M. 1979 *Physics Technol.* **10**, 259–265.
Cherns, D. 1974 *Phil. Mag.* **30**, 549–556.
Colliex, C. 1984 In *Advances in optical and electron microscopy* (ed. R. Barer & V. E. Cosslett), vol. 9, 65–177.
Cowley, J. M. 1984 *Proc. Mater. res. Soc. Symp.* **31**, 177.
Cowley, J. M., Albain, G. C., Hembree, G. G., Neilsen, P. E. H., Koch, F. A., Landry, J. D. & Shuman, H. 1975 *Rev. Scient Instrum* **46,** 826–829.
Cowley, J. M. & Kang, Z. C. 1983 *Ultramicroscopy* **11**, 131–140.
El-Gomati, M. M., Broomfield, J. P., Prutton, M. & Matthew, J. A. D. 1983 In *S.E.M. Proceedings* (Ed. O. Johari), pp. 1101–1106.
Fathers, D. J., Harland, C. J. & Venables, J. A. 1984 In *Inst. Phys. Conf. Ser.* no. 68 (EMAG 83), pp. 227–230.
Fathers, D. J. & Rez, P. 1984 In *Electron beam interactions with solids* pp. 193–208. Asilomar: S.E.M. Inc.
Futamoto, M., Hanbücken, M., Harland, C. J., Jones, G. W., Venables, J. A. 1985 *Surf. Sci.* **150**, 430–450.
Hanbücken, M., Futamoto, M. & Venables, J. A. 1984*b* *Surf. Sci.* **147**, 433–450.
Hanbücken, M., Neddermeyer, H. & Venables, J. A. 1984*a* *Surf. Sci.* **137**, L92–96.
Harland, C. J., Akhter, P. & Venables, J. A. 1981 *J. Phys.* E**14**, 175–182.
Harland, C. J. & Venables, J. A. 1985 *Ultramicroscopy* **17**, 9–20.
Heinemann, K., Osaka, T. & Poppa, H. 1983 *Ultramicroscopy* **12**, 9–18.
Hembree, G. G. & Cowley, J. M. 1979 In *S.E.M. proceedings* (ed. O. Johari) vol. 1, pp. 145–152.
Heraud, J. C. & Métois, J. J. 1980*a* *J. Cryst. Growth* **50**, 571–574.
Heraud, J. C. & Métois, J. J. 1980*b* *Acta metall.* **28**, 1789–1797.
Heraud, J. C. & Métois, J. J. 1983 *Surf. Sci.* **128**, 334–342.
Hovland, C. T., Mcdonald, N. C. & Gerlach, R. L. 1979 In *S.E.M. Proceedings* (ed. O. Johari), vol. 1, 213–218.
Howie, A. & Milne, R. H. 1985 *Ultramicroscopy* **18**, 427–433.
Hsu, T. 1983 *Ultramicroscopy* **11**, 167–172.
Hsu, T. & Cowley, J. M. 1985 *Proc. Mater. res. Soc. Symp.* **41**, 121.
Ichikawa, M. & Hayakawa, K. 1982 *Jap. J. appl. Phys.* **21**, 145–163.
Ichikawa, M., Doi, T., Ichihashi, M. & Hayakawa, K. 1984 *Jap. J. appl. Phys.* **23**, 913–920.
Ichinowkawa, T. & Ishikawa, Y. 1984*a* In *Inst. Phys. Conf. Ser.* no. 68 (EMAG 83), pp. 479–484.
Ichinowkawa, T. & Ishikawa, Y. 1984*b* *Ultramicroscopy* **15**, 193–204.
Iijima, S. & Ichihashi, T. 1985 *Jap. J. appl. Phys.* **24**, L125–L128.
Janssen, A. P., Akhter, P., Harland, C. J. & Venables, J. A. 1980 *Surf. Sci.* **93**, 453–470.
Janssen, A. P., Harland, C. J. & Venables, J. A. 1977 *Surf. Sci.* **62**, 277–292.
Jeanguillaume, C., Tence, M., Trebbia, P & Colliex, C. 1983 *S.E.M. Proceedings* (ed. O. Johari), vol. 2, 745–756.
Jones, G. W. & Venables, J. A. 1985 *Ultramicroscopy* **17**, 439–444.
Kanaya, K. & Ono, S. 1984 In *Electron beam interactions with solids*, pp. 69–98. Asilomar: S.E.M. Inc.
Kruit, P. & Read, F. H. 1983 *J. Phys.* E**16**, 313–324.
Langeron, J. P., Minel, L., Vignes, J. L., Bouquet, S., Pellerin, F., Lorang, G., Ailloud, P. & Le Hericy, J. 1984 *Surf. Sci.* **138**, 610–628.

PHILOSOPHICAL TRANSACTIONS OF THE ROYAL SOCIETY A MATHEMATICAL, PHYSICAL & ENGINEERING SCIENCES

Madey, T. E., Doering, D. L., Bertel, E. & Stockbauer, R. 1983 *Ultramicroscopy* **11**, 187–198.
Marks, L. D. 1983 *Phys. Rev. Lett.* **51**, 1000–1003.
Marks, L. D. & Smith, D. J. 1983 *Nature, Lond.* **303**, 316–317.
Métois, J. J. & LeLay, G. 1983 *Surf. Sci.* **133**, 422–442.
Osakabe, N., Yagi, K. & Honjo, G. 1980 *Surf. Sci.* **97**, 393–408.
Peacock, D. C. & Prutton, M. 1984 In *Inst. Phys. Conf. Ser.* no. 68 (EMAG 83), pp. 231–234.
Peacock, D. C., Prutton, M. & Roberts, R. 1984 *Vacuum* **34**, 497–507.
Pohl, D. W., Denk, W. & Lanz, M. 1984 *Appl. Phys. Lett.* **44**, 651–653.
Poppa, H. 1983 *Ulramicroscopy* **11**, 105–116.
Poppa, H. 1984 *Vacuum* **34**, 1081–1095.
Powell, C. J., Erickson, N. E. & Madey, T. E. 1982 *J. Electron Spectrosc. rel. Phen.* **25**, 87–118.
Prutton, M. 1982 *S.E.M. Proceedings* (ed. O. Johari), vol. 1, 83–91.
Schabes-Retchkiman, P. S. & Venables, J. A. 1981 *Surf. Sci.* **105**, 536–564.
Seiler, H. 1984 In *Electron beam interactions with solids*, pp. 33–42. Asilomar: S.E.M. inc.
Shannon, M. D., Eades, J. A., Meichle, M. E., Turner, P. S. & Buxton, B. F. 1984 *Phys. Rev. Lett.* **53**, 2125–2128.
Shimizu, N., Tanishiro, Y., Kobayashi, K., Takayanagi, K. & Yagi, K. 1985 *Ultramicroscopy* **17**, 453–461.
Sickafus, E. N. 1977 *Phys. Rev.* B**16**, 1436–1458.
Smith, D. J. 1985 In *Chemistry and physics of solid surfaces VI* (ed. R. Vanselow). Berlin: Springer. (In the press.)
Smith, D. J. & Marks, L. D. 1985*a* *Ultramicroscopy* **16**, 101–114.
Smith, D. J. & Marks, L. D. 1985*b* *Mater. Res. Symp.* **41**, 129–136.
Spence, J. C. H. 1976 In *Developments in electron microscopy and Analysis* (ed. J. A. Venables), pp. 257–260. London: Academic Press.
Spiller, G. D. T., Akhter, P. & Venables, J. A. 1983 *Surf. Sci.* **131**, 517–533.
Steeds, J. W. 1983 In *Introduction to analytical electron microscopy* (ed. J. J. Hren, J. I. Goldstein & D. C. Joy), pp. 387–422.
Takayanagi, K. 1982 *Ultramicroscopy* **8**, 145–162.
Tanishiro, Y., Takayanagi, K. & Yagi, K. 1983 *Ultramicroscopy* **11**, 95–102.
Venables, J. A. 1981 Ultramicroscopy **7**, 81–98.
Venables, J. A. 1982 In *Chemistry and physics of solid surfaces IV* (ed. R. Vanselow & R. Howe), pp. 123–147. Berlin: Springer.
Venables, J. A. 1983 *Vacuum* **33**, 701–705.
Venables, J. A. & Fathers, D. J. 1982 In *Proc. 10th. Int. Congr. on Electron Microscopy* (*Hamburg*), vol. 1, pp. 181–188.
Venables, J. A. & Janssen, A. P. 1978 In *Proc. 9th. Int. Congr. on Electron Microscopy* (*Toronto*), vol. 3, pp. 280–291.
Venables, J. A. & Janssen, A. P. 1980 *Ultramicroscopy* **5**, 297–315.
Venables, J. A., Janssen, A. P., Akhter, P., Derrien, J. & Harland, C. J. 1980 *J. Microsc.* **118**, 351–365.
Venables, J. A., Seguin, J. L., Suzanne, J. & Beinfait, M. 1984*b* *Surf. Sci.* **145**, 345–363.
Venables, J. A., Spiller, G. D. T., Fathers, D. J., Harland, C. J. & Hanbücken, M. 1983 *Ultramicroscopy* **11**, 149–156.
Venables, J. A., Spiller, G. D. T. & Hanbücken, M. 1984*a* *Rep. Prog. Phys.* **47**, 399–459.
Yagi, K. 1982 In *S.E.M. Proceedings* (ed. O. Johari), vol. 4, 1421–1428.
Yagi, K., Takayanagi, K. & Honjo, G. 1982 In *Crystals, growth, properties and applications*, vol. 7, pp. 48–74. Berlin: Springer.

PHILOSOPHICAL TRANSACTIONS OF THE ROYAL SOCIETY A MATHEMATICAL, PHYSICAL & ENGINEERING SCIENCES

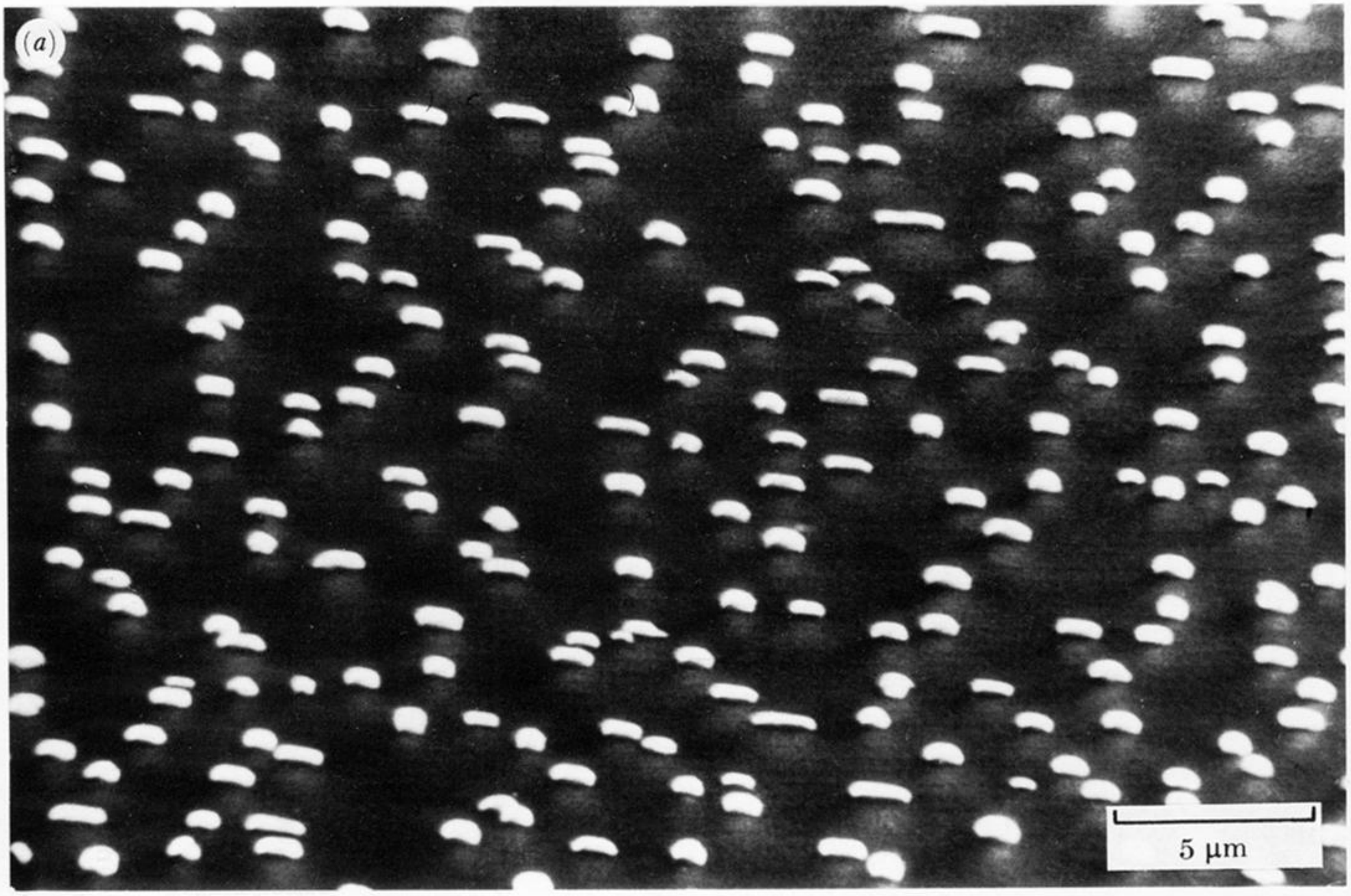

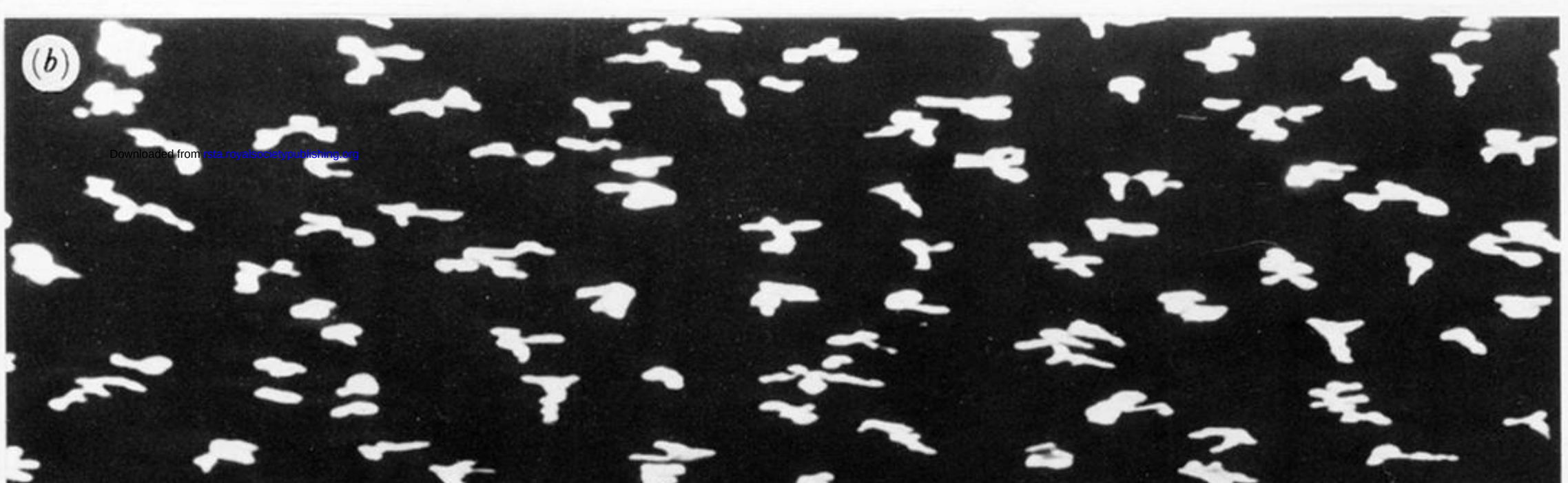

FIGURE 1. S.e.m. pictures of island densities and crystal shapes for (*a*) Ag/Si(100) at $T = 823$ K and (*b*) Ag/Si(111) at $T = 673$ K. Note the higher density on Si(100) despite the higher T, and the difference of shape between the two surfaces. S.e.m. pictures taken at a beam voltage $E_0 = 30$ keV, at $\theta_0 = 70°$ (Hanbücken *et al.* 1984*b*).

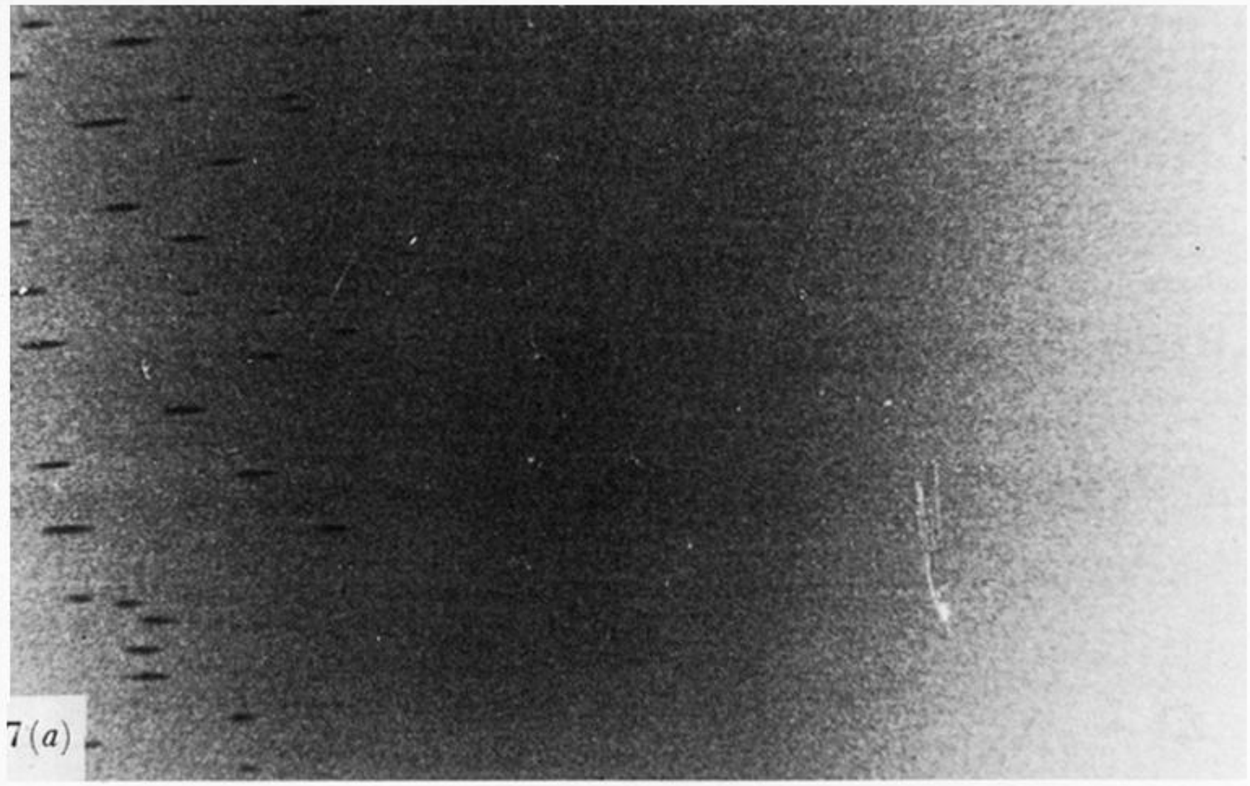

FIGURE 7. Biased secondary-election images of 5 m.l. Ag/W(110), deposited past a mask edge at $T = 673$ K at 0.5 m.l. per minute; observations at $E_0 = 30$ keV, $\theta_0 = 70°$: (*a*) zero bias with the Ag islands showing dark, where the layers are essentially invisible; (*b*) $V_b = -200$ V, showing the islands bright and the 1 and 2 m.l. steps clearly visible (Jones & Venables 1985).

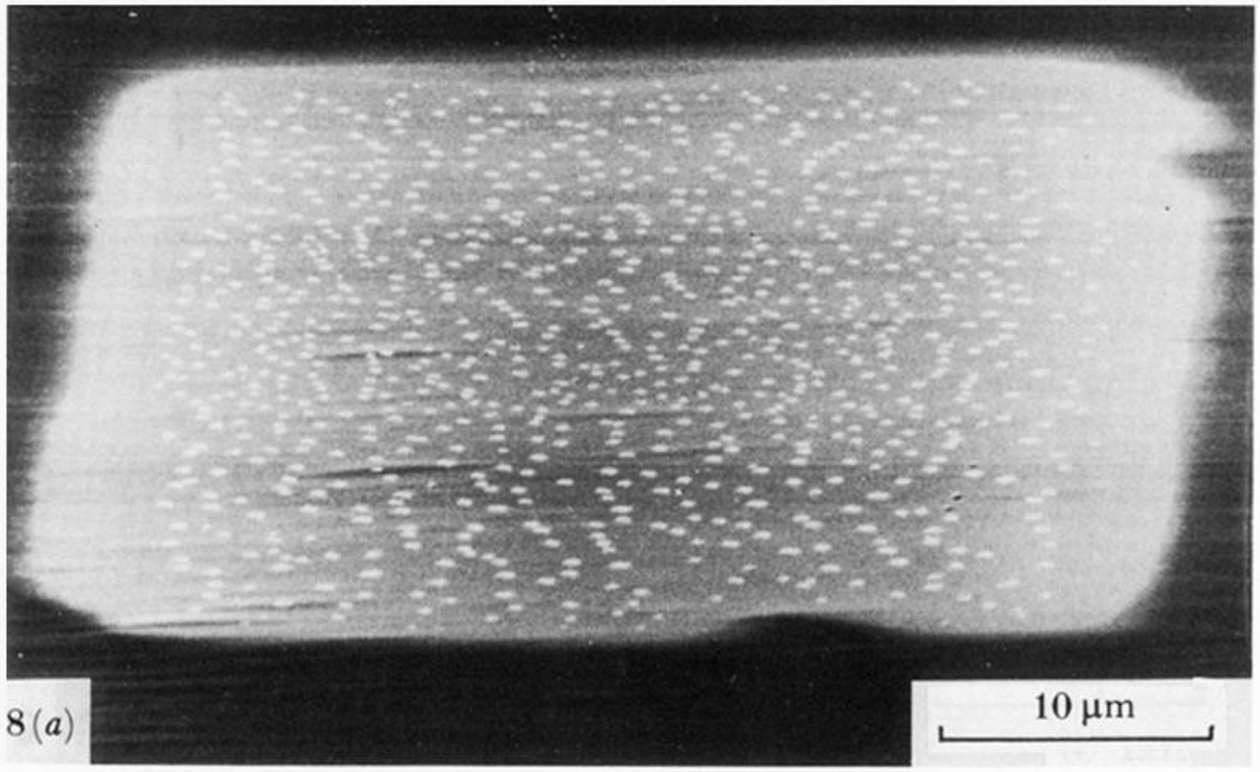

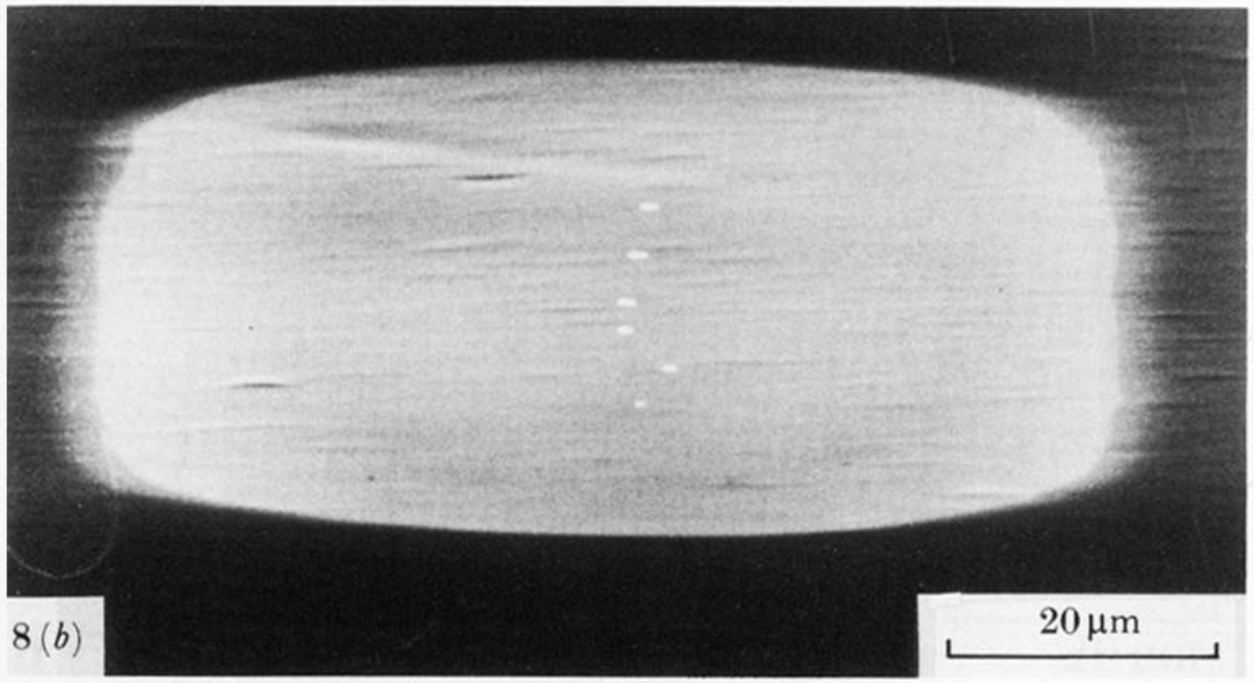

FIGURE 8. Competition between surface diffusion and nucleation on an individual masked area for Ag/W(110). Five monolayers were deposited through a mask hole 32 μm wide by 100 μm long, observed at $E_0 = 30$ keV: (*a*) $T = 573$ K, $\theta_0 = 76°$, diffusion width about 4 μm; (*b*) $T = 733$ K, $\theta_0 = 68°$, diffusion width about 38 μm; (Jones & Venables 1985).

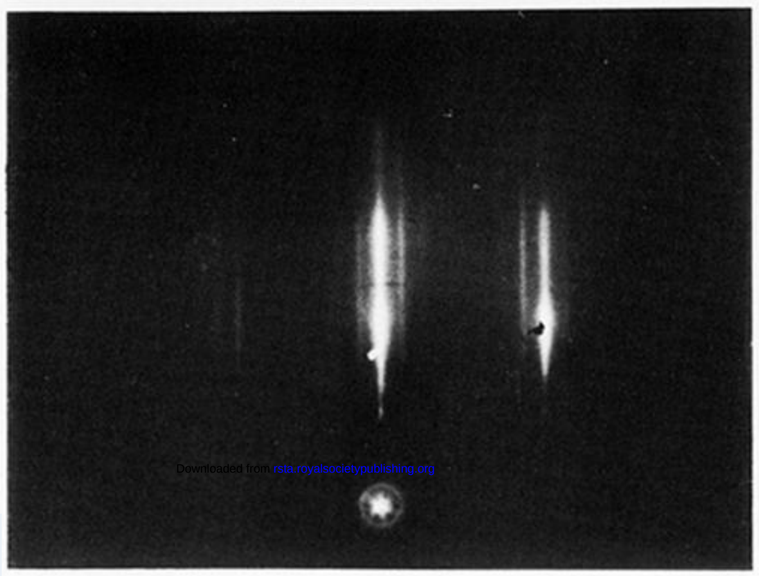

(a)

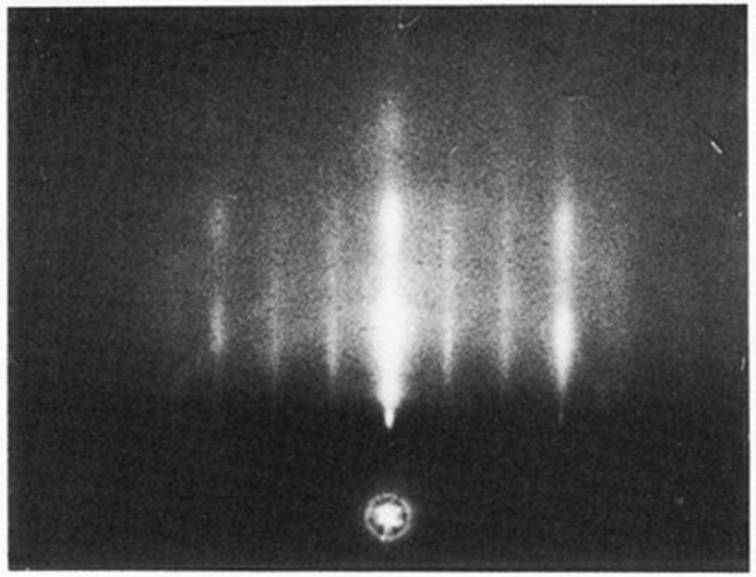

(b)

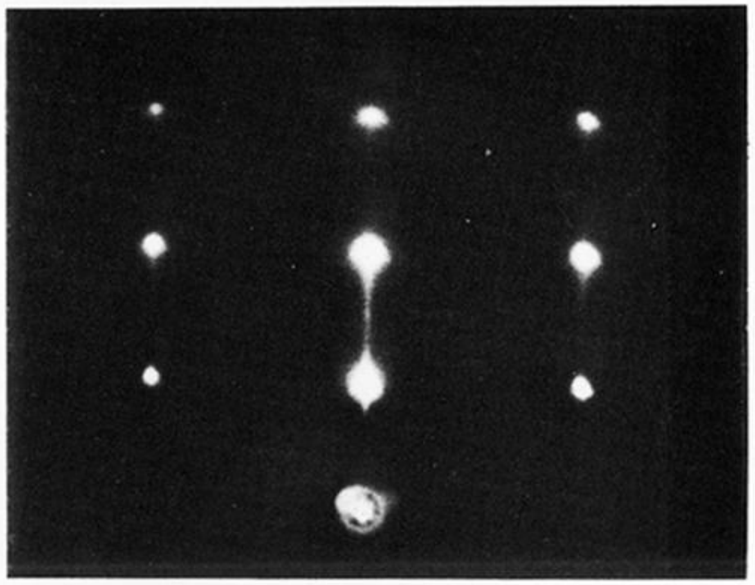

(c)

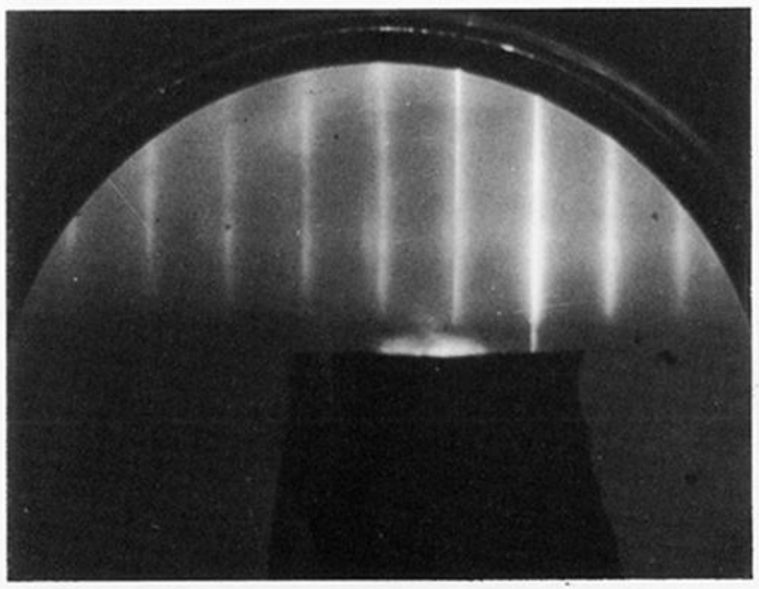

(d)

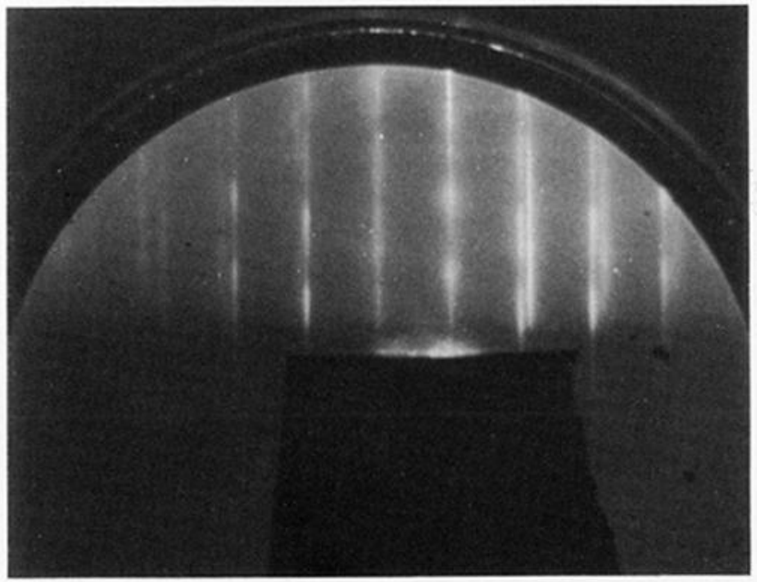

(e)

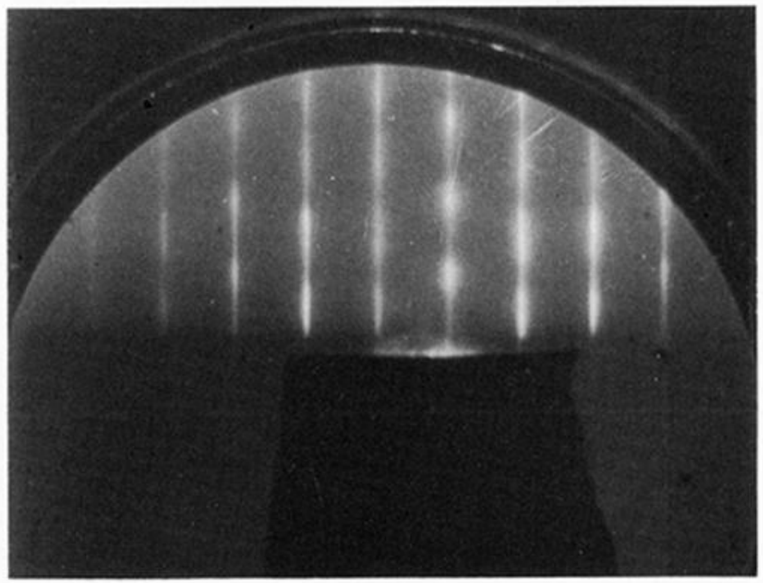

(f)

FIGURE 11 R.h.e.e.d. patterns from Ag/Si(111) and Ag/W(110). (*a*)–(*c*) Ag/Si(111) from Venables *et al.* (1980): (*a*) clean Si(111) (7 × 7) veiwed along [11$\bar{2}$]; (*b*) the $\sqrt{3} \times \sqrt{3}$ Ag intermediate layer structure; (*c*)transmission through Ag(111) islands in $\langle 11\bar{2} \rangle$ orientation. (*d*)–(*f*): Ag/W(11) from Jones & Venables (1985): (*d*) clean W(110) viewed along [001]: (*e*) W(110) + 2 m.l. Ag in the 'selvedge' region of figure 7; (*f*) Ag island region showing modulated streaks, corresponding to twinned $\langle 1\bar{1}0 \rangle$ directions.

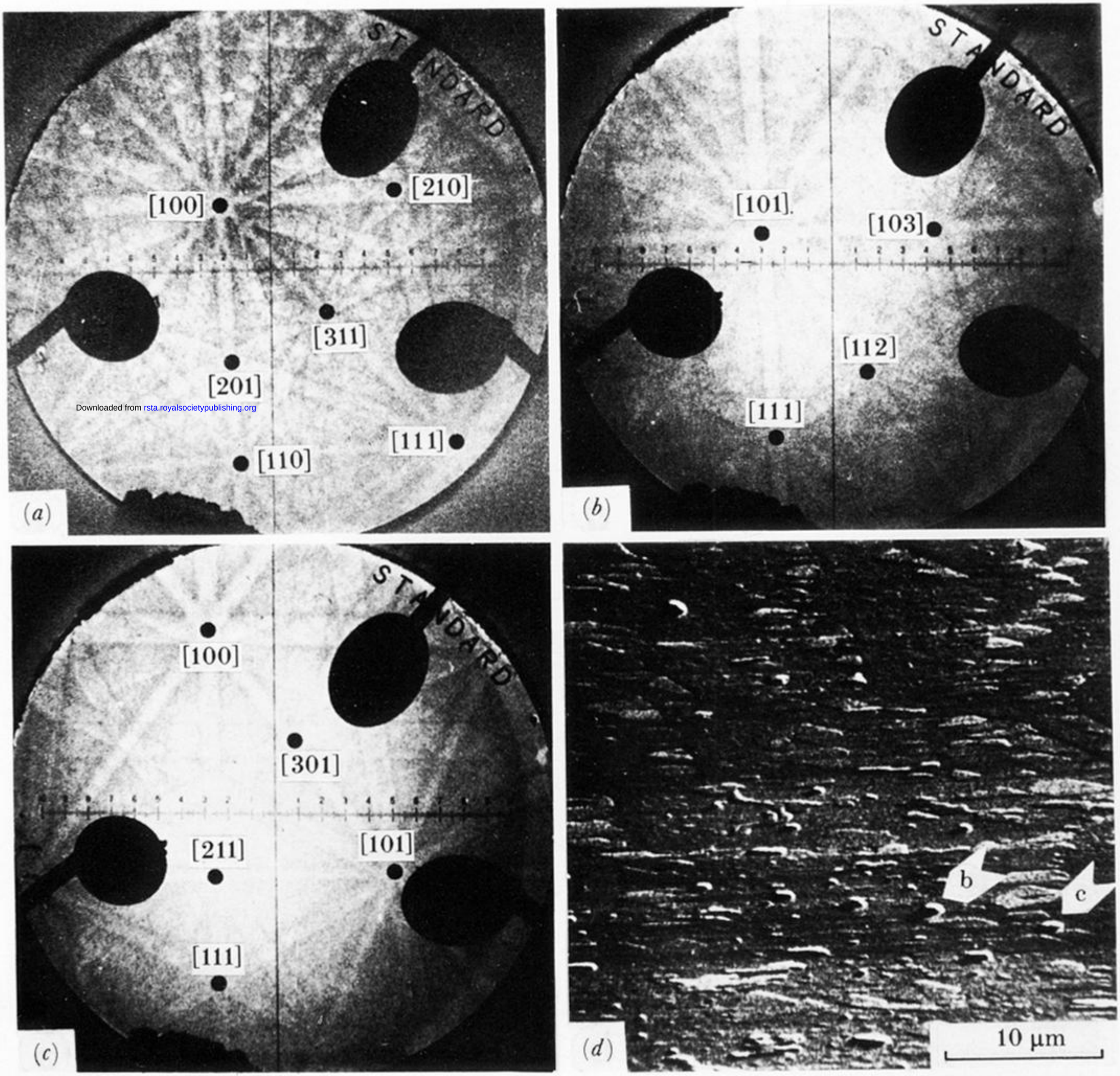

FIGURE 12. Electrons back-scattering patterns from Ag/W(110): (*a*) W(110) substrate patterns; (*b*) (111) oriented Ag crystal; (*c*) similar (111) crystal in twin-related orientation; (*d*) s.e.m. picture at $\theta_0 = 75°$, showing Ag crystals B and C whose patterns are seen in (*b*) and (*c*) respectively (Harland *et al.* 1981).

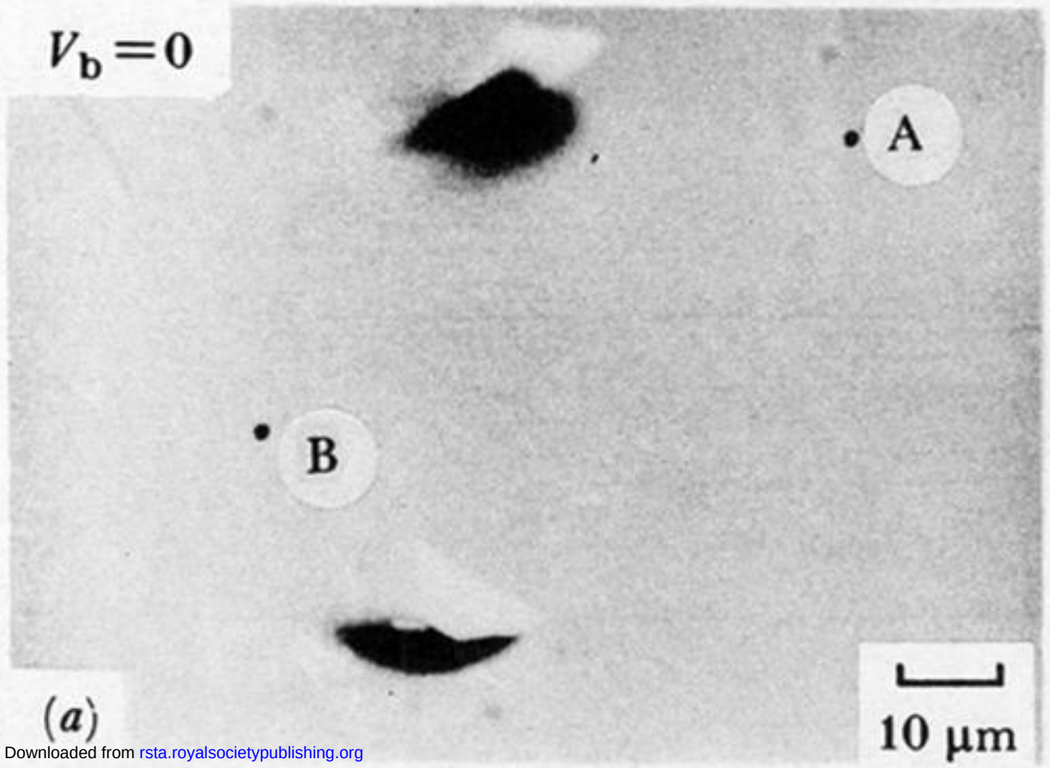

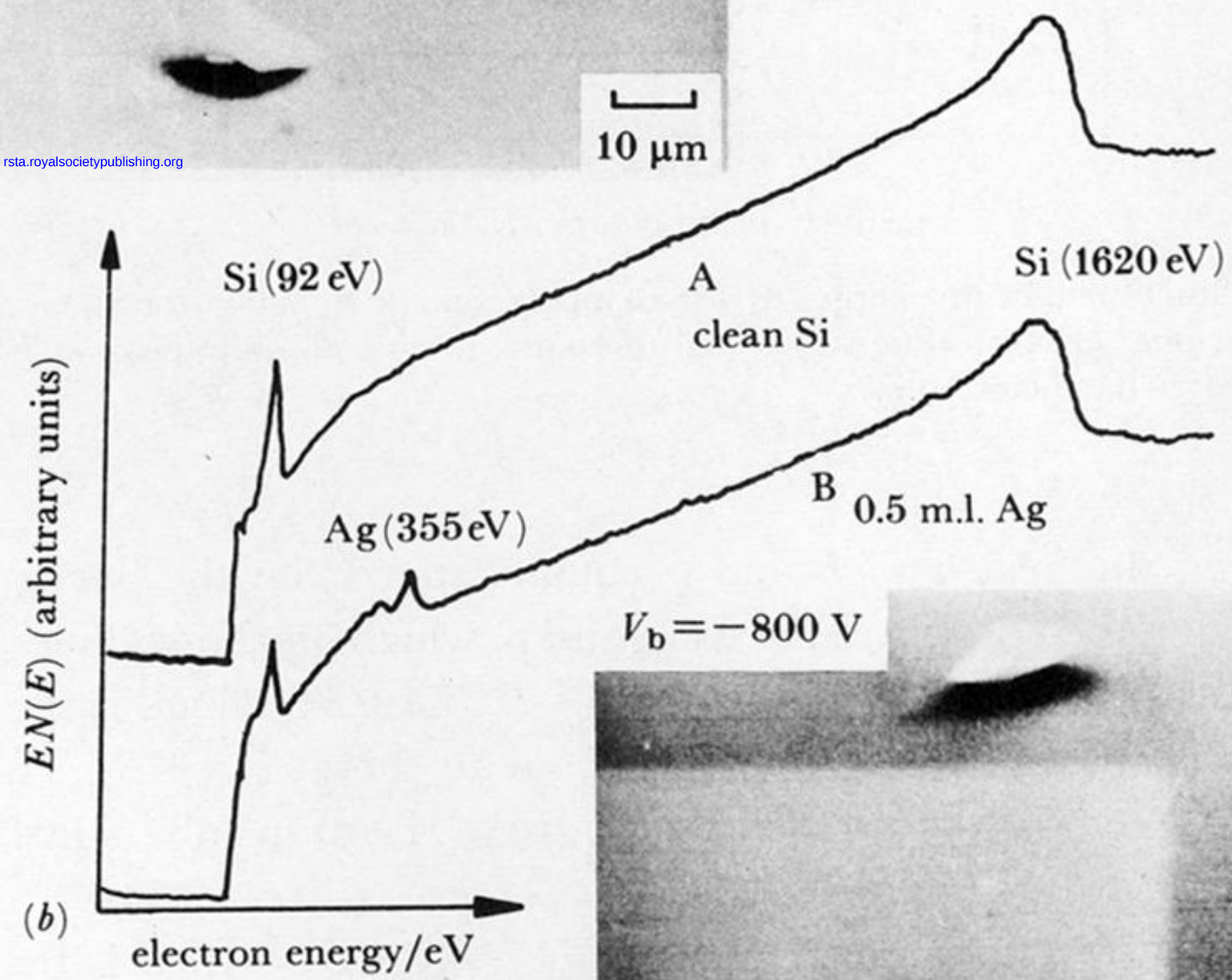

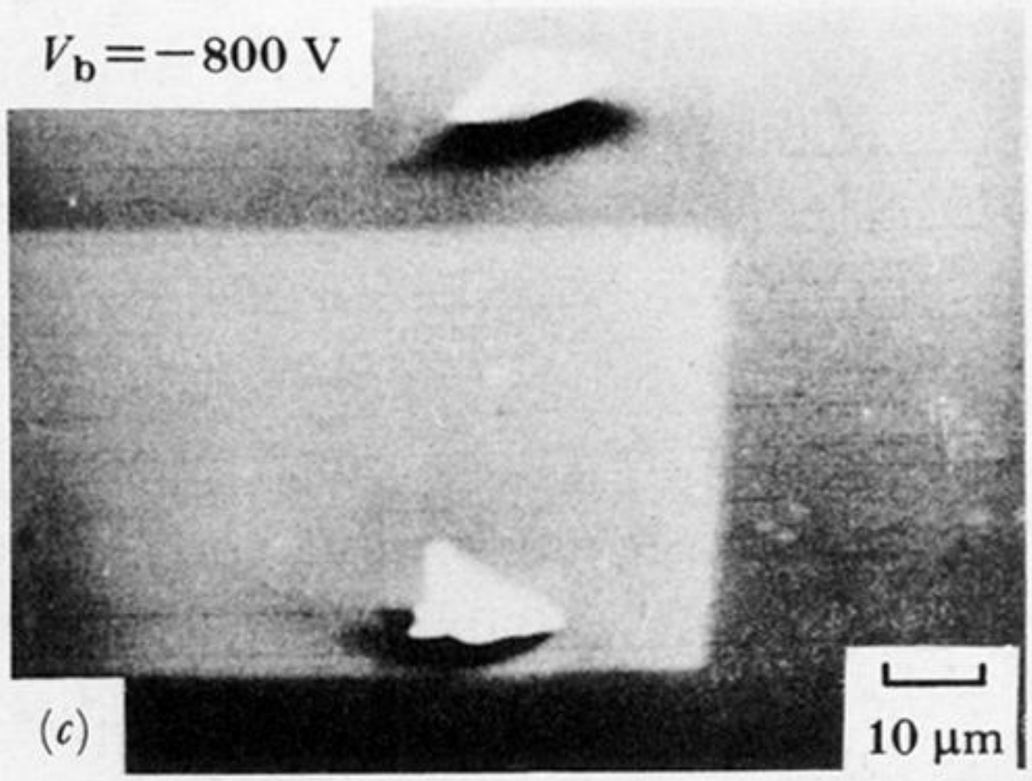

FIGURE 6. Demonstration of biased secondary-electron imaging for 0.5 m.l. Ag/Si(100), deposited at room temperature. (*a*) zero bias, showing dust-particle markers; (*b*) Auger spectra from points A and B in (*a*); (*c*) sample bias $V_b = -800$ V, showing the masked area of Ag deposited (Futamoto *et al.* 1985).